Supporting Information for

Pd loaded and covalent-organic frameworks involved chitosan aerogels and their application for continuous flow-through aqueous CBs decontamination

Fei Li,[†a] Luo-Gang Ding,[†a] Bing-Jian Yao,[*a] Ning Huang,[b] Jiang-Tao Li,[a] Qi-Juan Fu,[a] Yu-Bin Dong[*a]

[a] College of Chemistry, Chemical Engineering and Materials Science, Collaborative Innovation Center of Functionalized Probes for Chemical Imaging in Universities of Shandong, Key Laboratory of Molecular and Nano Probes, Ministry of Education, Shandong Normal University, Jinan 250014, P. R. China.

[b] Department of Chemistry, Texas A&M University, College Station, Texas 77843-3255, United States.

*E-mail: yaobingjian1986@163.com, yubindong@sdnu.edu.cn

[†]Dual Contributors

Content

1. Materials and instrumentation

All the chemicals were obtained from commercial sources (Acros) and used without further purification. ^{1}H NMR data were collected on a Bruker Avance-400 spectrometer. Chemical shifts are reported in δ relative to TMS. Infrared (IR) spectrum were obtained in the 400-4000 cm^{-1} range using a Bruker ALPHA FT-IR Spectrometer. Elemental analyses for C, H, and N were performed on a Perkin-Elmer model 2400 analyzer. Powder X-ray diffraction (PXRD) pattern was obtained on D8 ADVANCE with Cu Kα radiation (λ = 1.5405 Å). The scanning electron microscopy (SEM) micrographs were recorded on a Gemini Zeiss Supra TM scanning electron microscope equipped with energy-dispersive X-ray detector (EDS). The transmission electron microscopy (TEM) was performed on a JEM-1400 electron microscope (JEOL) operated at an accelerating voltage of 120 kV. The N_2 adsorption isotherms were performed on an ASAP 2020/TriStar 3000 (Micromeritics) at 77 K. ICP measurement was performed on an IRIS Interpid (II) XSP and NU AttoM. X-ray photoelectron spectroscopy (XPS) data were obtained with an PHI 5000 Versaprobe II (VP-II) electron spectrometer from Ulvac-Phi using 300 W Al Kα radiation. The base pressure for the measurement was approximately 3×10^{-9} mbar. The binding energies were referenced to the C_{1s} line at 284.8 eV from adventitious carbon. XPS results were obtained by analyzing the elements present in the air-facing side of the specimen films with a 90° to the electron beam. Gas chromatography (GC) analysis was performed on an Agilent 7890B GC. Structural modeling of COF was generated using the Materials Studio (ver. 7.0) suite of programs. Molecular geometry optimization was performed with MS DMol3 module. The compressive mechanical property of the aerogel was investigated using a UTM4000 instrument from shenzhen suns Technology co., ltd. The axial direction of the cylindrical aerogel (24 mm in height, 21 mm in diameter) was compressed at 5 mm min^{-1}.

2. Synthesis and characterization of TpPa-1, TpPa-NO_2, NUS-2, TpTe-1, and Pd@TpTe-1

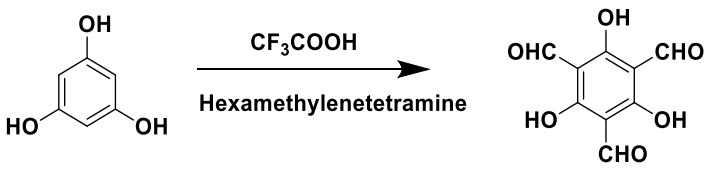

Scheme S1. Synthesis of 1,3,5-triformylphloroglucinol.

Synthesis of 1,3,5-triformylphloroglucinol (Tp). A mixture of hexamethylenetetraamine (7.42 g, 52.9 mmol), dried phloroglucinol (3.0 g, 23.8 mmol) in 45 mL of trifluoroacetic acid was heated at 100°C for 2.5 h in N_2 atmosphere. After addition of 75 mL of 3 M HCl, the mixture was heated at 100°C for additional 1 h. After cooling to room temperature, the solution was filtered through Celite, extracted with dichloromethane, and dried over anhydrous magnesium sulfate. Rotary evaporation of the solution afforded 1,3,5-triformylphloroglucinol as an off-white powder (0.54 g, 18 % yield). ^{1}H NMR (400 MHz, $CDCl_3$, δ, ppm) 14.128 (s, 3H),10.156 (s, 3H). ESI-MS: calcd for $[C_9H_6O_6\text{-}H]$ *m/z* 209.01, found *m/z* 209.01; FTIR (KBr, cm^{-1}): 2887(w), 1643(s), 1606(m), 1434(s), 1251(m), 1192(s), 968(s), 873(m), 788(m), 608(s). ^{13}C NMR (400 MHz, DMSO-d_6, δ, ppm): 192, 173, 104.

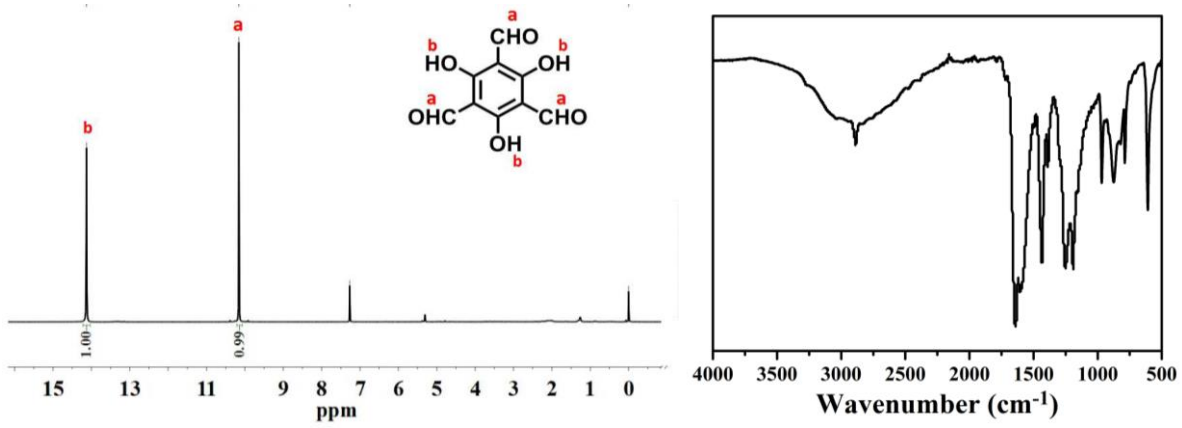

Fig. S1 ^{1}H-NMR (in $CDCl_3$) and IR spectra of 1,3,5-triformylphloroglucinol.

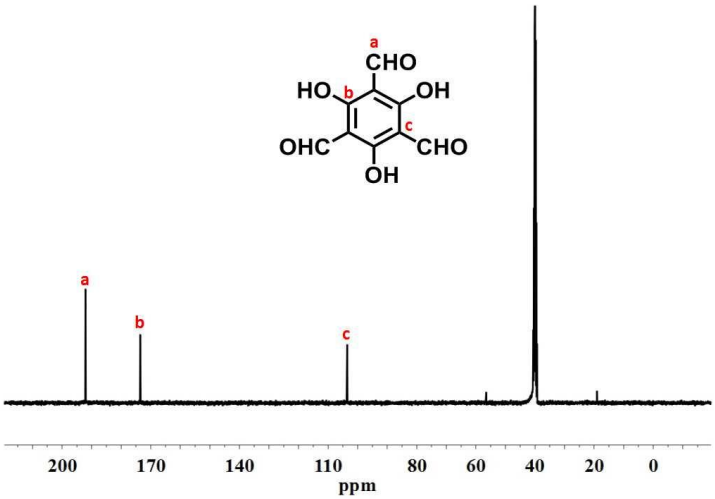

Fig. S2 ^{13}C-NMR spectrum (in DMSO-d_6) of 1,3,5-triformylphloroglucinol.

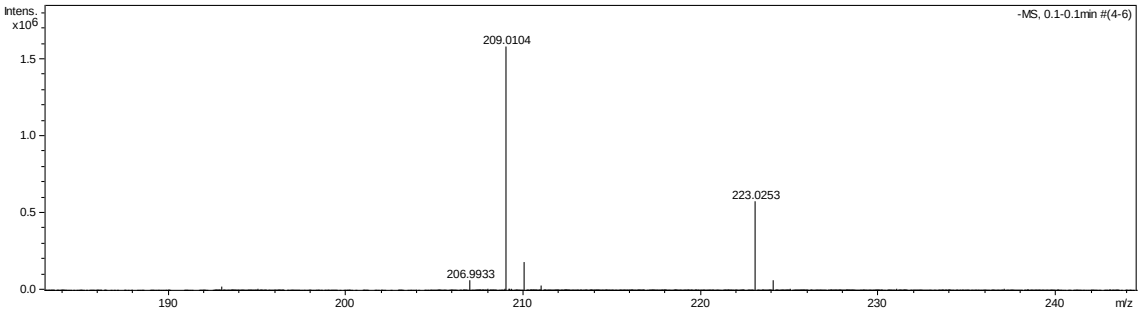

Fig. S3 Mass spectrum (MS) of 1,3,5-triformylphloroglucinol. Calcd for [$C_9H_6O_6$-H], *m/z* 209.01; found, *m/z* 209.01.

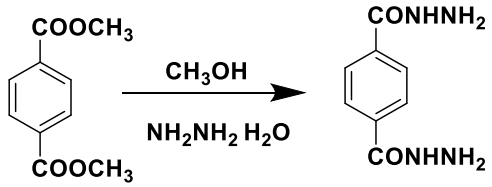

Scheme S2. Synthesis of terephthalohydrazide.

Synthesis of terephthalohydrazide. Dimethyl terephthalate (2.8 g, 14.5 mmol) was dissolved in 58 mL of methanol and 8.5 mL of hydrazine hydrate. The mixture was refluxed for 15 h. After cooling, white crystals was formed and isolated by filtration, and thoroughly washed with cold methanol to generate terephthalohydrazide (2.11 g, 75 % yield). ^{1}H NMR (400 MHz, DMSO-d_6, δ, ppm), 9.89 (s, 2H), 7.87 (s, 4H), 4.55 (s, 4H). ESI-MS: calcd for [$C_8H_{10}N_4O_2$+H], m/z 195.08; found, m/z 195.0881. FTIR (KBr, cm^{-1}): 3313(s), 1606(s), 1542(s), 1491(s), 1341(s), 1292(m), 1103(m), 927(s), 888(m), 737(w), 636(m). ^{13}C NMR (400 MHz, DMSO-d_6, δ, ppm): 165, 136, 128.

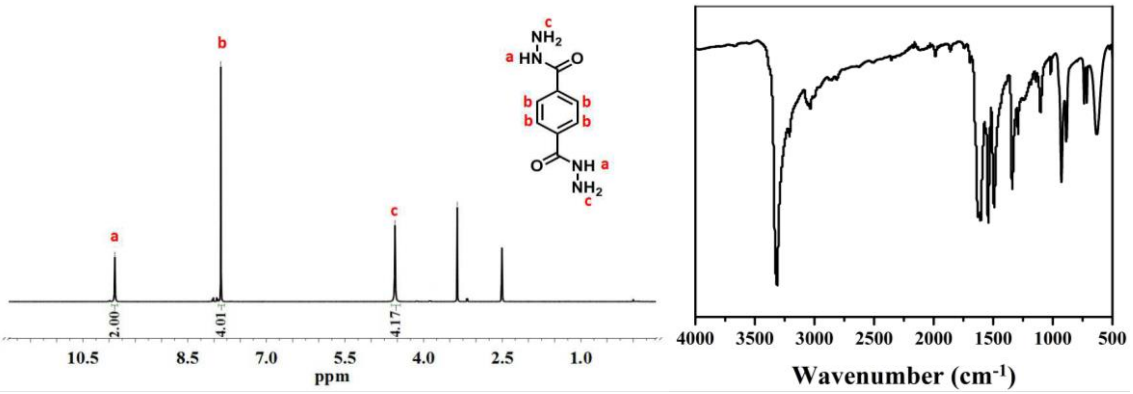

Fig. S4 ^{1}H-NMR (in DMSO-d_6) and IR spectra of terephthalohydrazide.

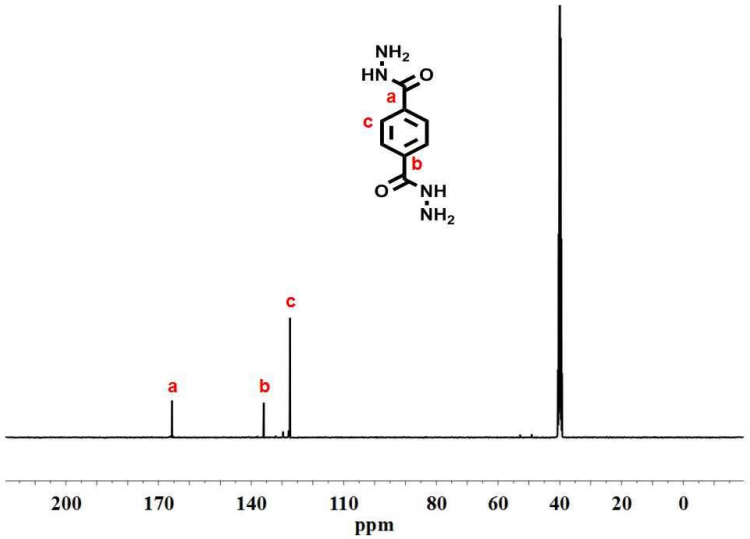

Fig. S5 ^{13}C-NMR (in DMSO-d_6) spectrum of terephthalohydrazide.

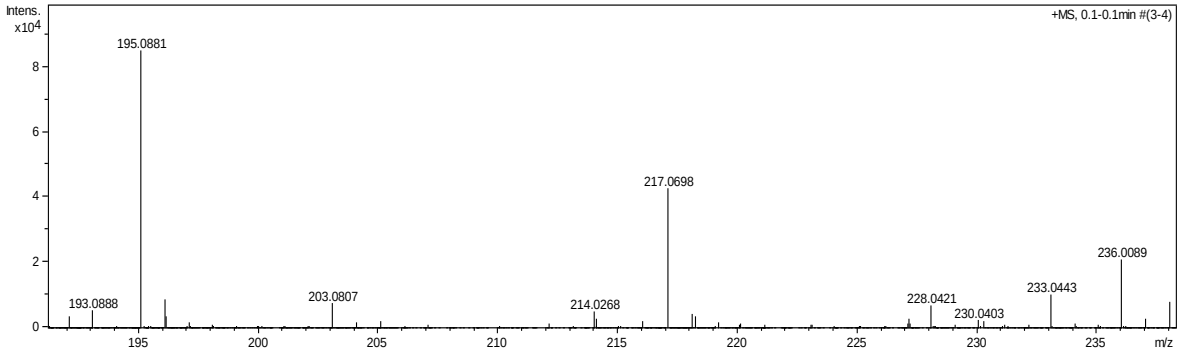

Fig. S6 Mass spectrum (MS) of terephthalohydrazide, calcd for [$C_8H_{10}N_4O_2$+H], *m/z* 195.08; found, *m/z* 195.0881.

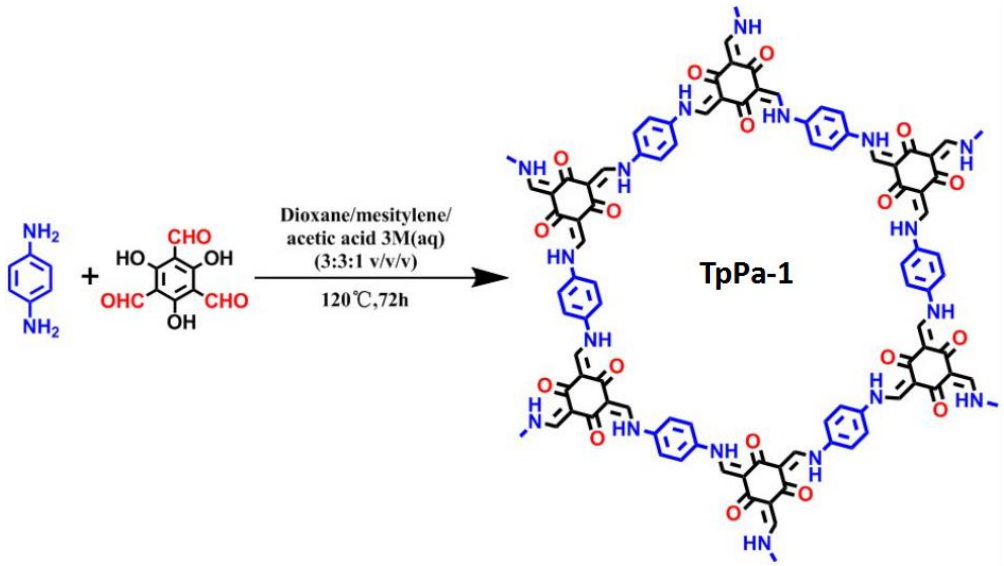

Scheme S3. Synthesis of **TpPa-1**.

Synthesis of TpPa-1. TpPa-1 was synthesized according to the reported procedure.[1] A mixture of

1,3,5-triformylphloroglucinol (0.3 mmol, Tp), 1,4-phenelynediamine (0.45 mmol, Pa), mesitylene (1.5 mL), 1,4-dioxane (1.5 mL), and aqueous acetic acid (0.5 mL of 3 M) in a tube was sonicated for 10 min in order to get a homogeneous dispersion. The tube was then flash frozen at 77 k (liquid N_2 bath) and degassed by three freeze-pump-thaw cycles. After that, the mixture was heated at 120 °C in the sealed tube for 3 days. The obtained dark red colored precipitate was collected by centrifugation, and then washed with acetone. After solvent exchanged with acetone and dried at 100 °C under vacuum for 12 h to afford the corresponding **TpPa-1** in 82 % yield. Elemental analysis: cald for $(C_{16}H_{13}N_3O_3)_n$ (%): C 65.06, H 4.4, N 14.23; found: C 64.12, H 4.27, N 14.17. FTIR (KBr, cm^{-1}): 3340 (m), 2973 (m), 2883 (w), 1583 (s), 1519 (m), 1452 (s), 1284 (s), 1255 (s), 1090 (s), 1049 (s), 990 (w), 880 (m), 825 (w). Solid-state ^{13}C CP-MAS NMR (500 MHz, δ, ppm): 163, 146, 133, 128, 100; PXRD pattern (2*θ*): The peak at 4.5, 8.5, 12.5, and 26.8° attributed to the (100), (200), (210), and (001) reflection planes, respectively.

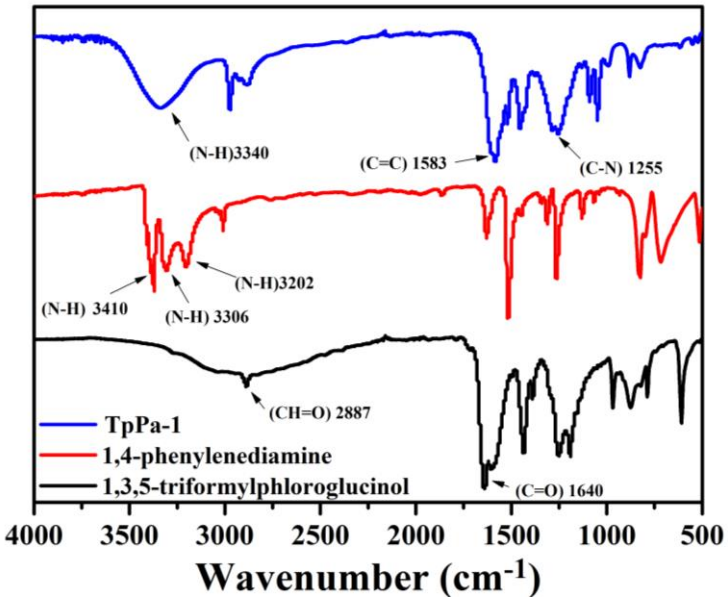

Fig. S7 IR spectra of **TpPa-1**, 1,3,5-triformylphloroglucinol, and 1,4-phenelynediamine. The characteristic stretching vibrations at 3410 cm^{-1} for N-H bond and at 1640 cm^{-1} for C=O groups in the starting materials disappeared after the reaction. Meanwhile, the strong peak at 1583 cm^{-1} for the C=C stretching present in the keto form was observed.

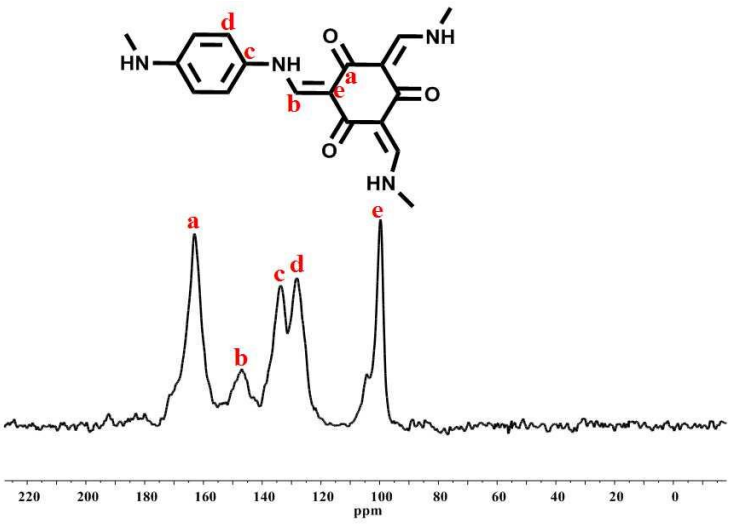

Fig. S8 Solid-state ^{13}C-MAS NMR spectrum of **TpPa-1**. The peaks at 163 and 100 ppm correspond to the ring in keto form. The peak at 146 ppm can be assigned to the C=*C*-N groups. The peaks at 133 and 128 ppm belongs to the phenyl ring.

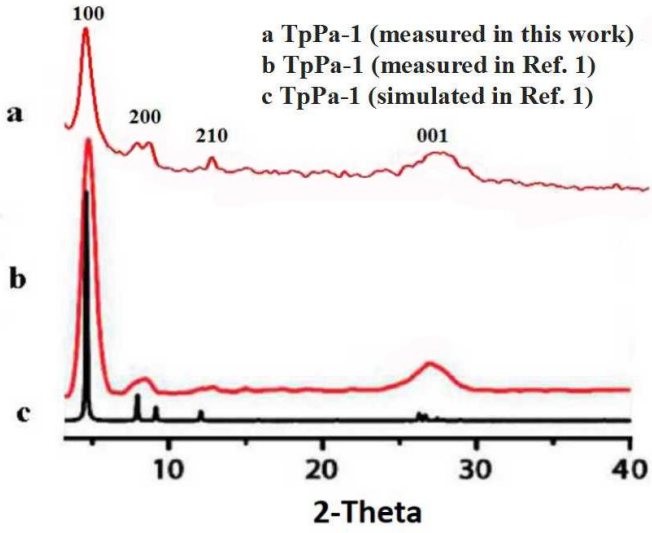

Fig. S9 The measured PXRD patterns of **TpPa-1** (a), which were well consistent with the reported results (b and c). The peak at 4.5, 8.5, 12.5, and 26.8° attributed to the (100), (200), (210), and (001) reflection planes, respectively.

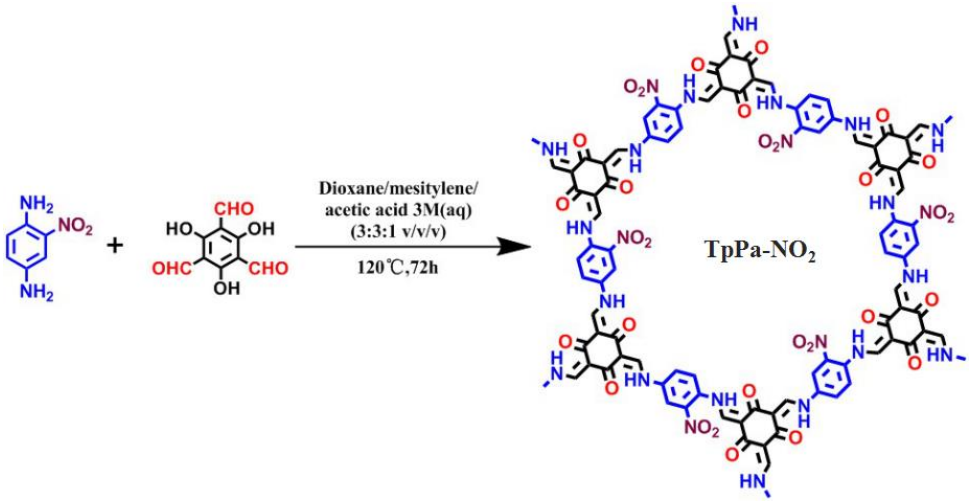

Scheme S4. Synthesis of **TpPa-NO_2**.

Synthesis of TpPa-NO_2. TpPa-NO_2 was synthesized according to the reported procedure.[2] A mixture of 1,3,5-triformylphloroglucinol (0.3 mmol, Tp), 2-nitro-1,4-phenelynediamine (0.45 mmol, Pa-NO_2), mesitylene (1.5 mL), 1,4-dioxane (1.5 mL), and aqueous acetic acid (0.5 mL, 3 M) in a tube was sonicated for 10 min in order to get a homogeneous dispersion. The tube was then flash frozen at 77 K (liquid N_2 bath) and degassed by three freeze-pump-thaw cycles. Then, the mixture was heated at 120 °C for 3 days. A dark red colored precipitate was collected by centrifugation, and then washed with acetone. After solvent exchanged with acetone and dried at 100 °C under vacuum for 12 h to generate the corresponding **TpPa-NO_2** in 76 % yield. Elemental analysis: cald for $(C_{16}H_{12}N_4O_5)_n$ (%): C 56.46, H 3.5, N 16.4; found: C 54.51, H 3.23, N 16.67. FTIR (KBr, cm^{-1}): 3474 (w), 3361 (m), 2972 (w), 1604 (s), 1524 (s), 1450 (m), 1289 (m), 1254 (s), 1095 (w), 992 (w), 819 (m). Solid-state ^{13}C CP-MAS NMR (500 MHz, δ, ppm): 184, 145, 135, 130, 122, 107, 101. PXRD pattern (2θ): The peak at 4.7, 8.1, 11.1, and 27° attributed to the (100), (200), (210), and (001) reflection planes, respectively.

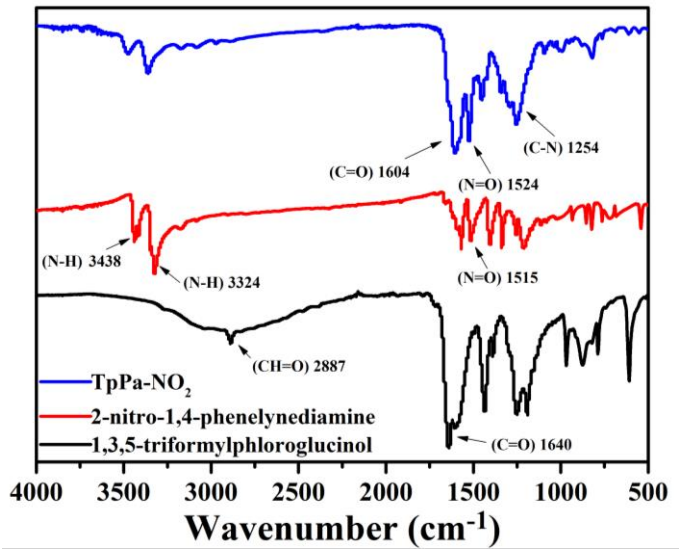

Fig. S10 IR spectra of **TpPa-NO$_2$**, 1,3,5-triformylphloroglucinol, and 2-nitro-1,4-phenelynediamine. The characteristic stretching vibrations at 1640 cm^{-1} for C=O groups in the starting materials disappeared after the reaction. Meanwhile, the strong peak at 1604 cm^{-1} for the C=C stretching present in the keto form was observed. Additionally, a peak appears exactly at 1524 cm^{-1} in **TpPa-NO$_2$** corresponds to the -NO$_2$ groups and confirms its presence in the framework.

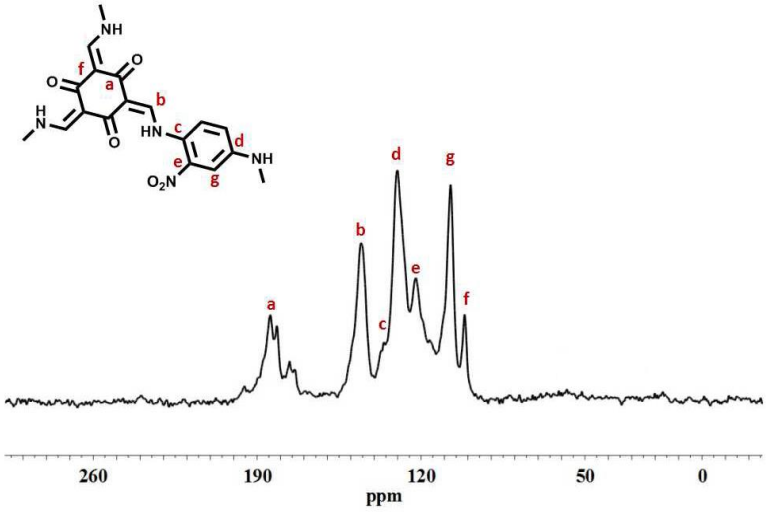

Fig. S11 Solid-state ^{13}C-MAS NMR spectrum of **TpPa-NO$_2$**. The peaks at 184 and 101 ppm correspond to the ring in keto form. The peak at 145 ppm can be assigned to the C=*C*-N groups. The peaks at 135, 130, 122, and 107 ppm belongs to the phenyl ring.

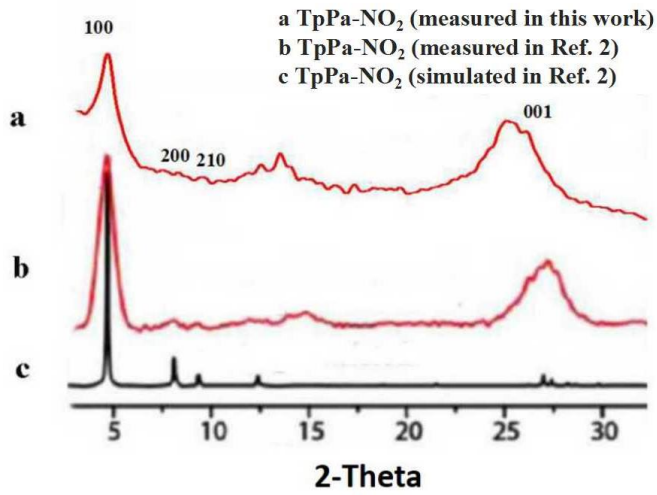

Fig. S12 The measured PXRD patterns of **TpPa-NO₂** (a), which were well consistent with the reported results (b and c). The peak at 4.7, 8.1, 11.1, and 27° attributed to the (100), (200), (210), and (001) reflection planes, respectively.

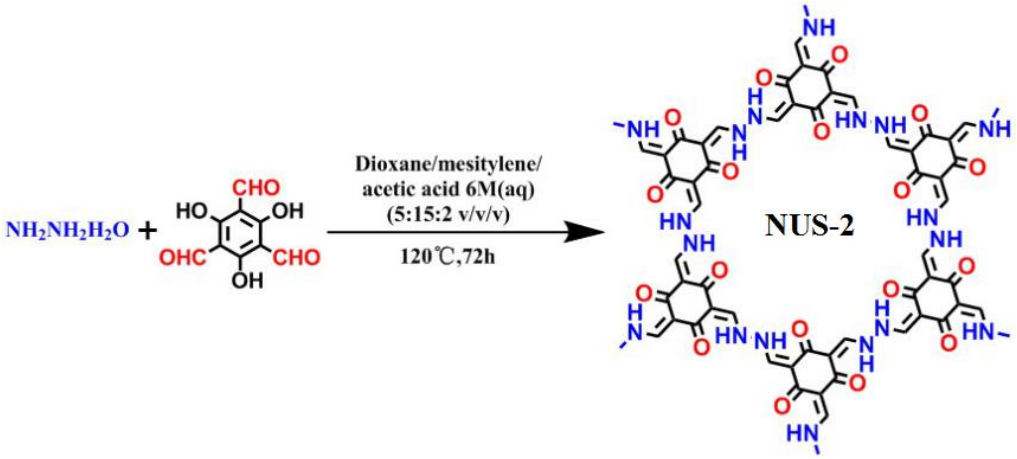

Scheme S5. Synthesis of **NUS-2**.

Synthesis of NUS-2. NUS-2 was synthesized according to the reported procedure.[3] 0.15 mmol of hydrazine and 0.10 mmol of 1,3,5-triformylphloroglucinol (Tp) were weighed into a glass pressure tubing. After addition of 1,4-dioxane (1.0 mL), mesitylene (3.0 mL), and 0.4 mL of 6.0 M aqueous acetic acid, the tube was then flash frozen at 77 K (liquid N_2 bath) and degassed by three freeze-pump-thaw cycles. The tube was sealed off and then heated at 120 °C for 3 days. A yellow colored precipitate was isolated by centrifugation and washed with acetone (3×10 mL) and THF (3×10 mL), dried at 80 °C under vacuum for 24 h to yield **NUS-2** as yellow powder in 86 % yield. Elemental analysis: cald for $(C_{10}H_9N_3O_3)_n$ (%): C 54.48, H 4.1, N 19.2; found: C 54.39, H 3.89, N 18.50. FTIR (KBr, cm^{-1}): 2998 (w), 1589 (s), 1456 (m), 1271(s), 1182 (s), 983 (w), 818 (m), 784 (m), 612 (m). Solid-state ^{13}C CP-MAS NMR (500 MHz, δ, ppm): 180, 171, 157, 100. PXRD pattern (2θ):

The peak at 6.9, 11.8, and 26.8° attributed to the (100), (200), and (001) reflection planes, respectively.

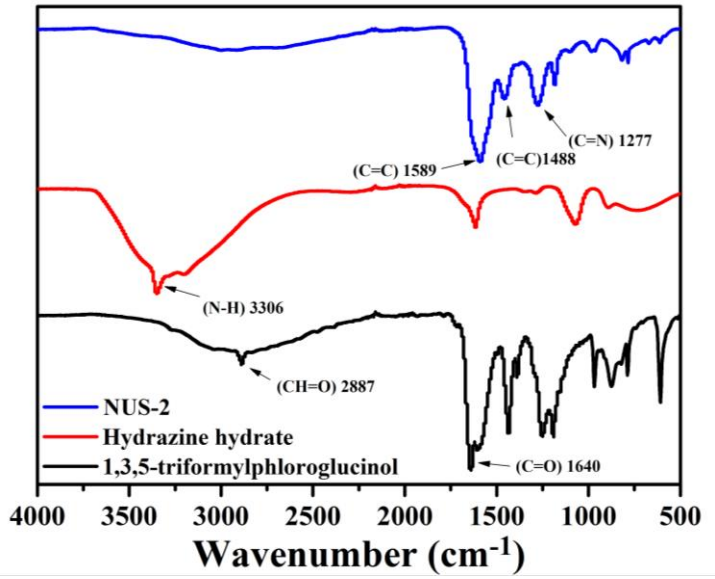

Fig. S13 IR spectra of **NUS-2**, 1,3,5-triformylphloroglucinol, and hydrazine hydrate. The characteristic stretching vibration at 3306 cm^{-1} for N-H groups and 1640 cm^{-1} for C=O groups in the starting materials disappeared after the reaction. Meanwhile, a series of new characteristic stretching bands at 1589, 1488, and 1277 cm^{-1} for **NUS-2** arising from the C=O, C=C, and C=N stretching bands, respectively, were observed indicating the successful condensation reaction.

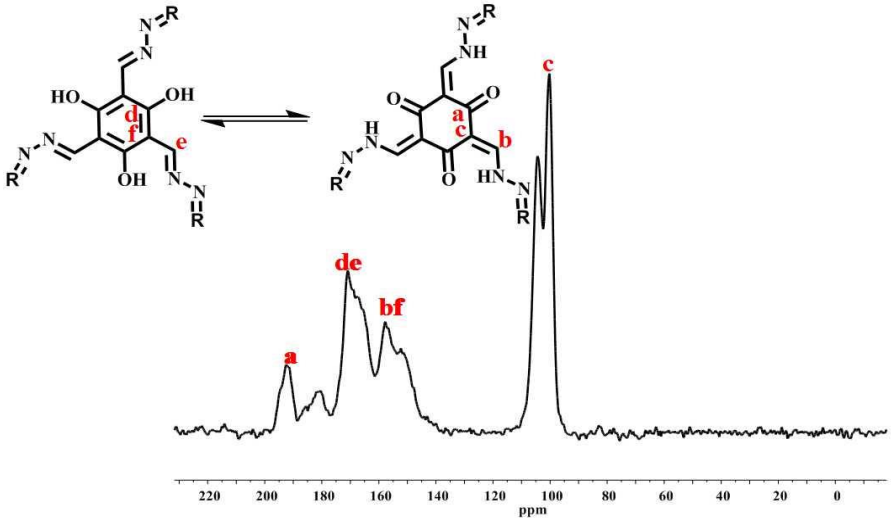

Fig. S14 Solid-state ^{13}C-MAS NMR spectrum of **NUS-2**. The peak at 180 ppm could be ascribed as the carbonyl carbon [*C*=O] of the keto form. The peak at 157 ppm confirms the presence of the *C*-N and *C*-*C* bond. The resonance at 171 ppm is assigned to both the *C*=N and the enol carbon [*C*-O] form. The peak at 100 ppm correspond to the sp^2 hybridized olefinic carbon *C*=*C*.

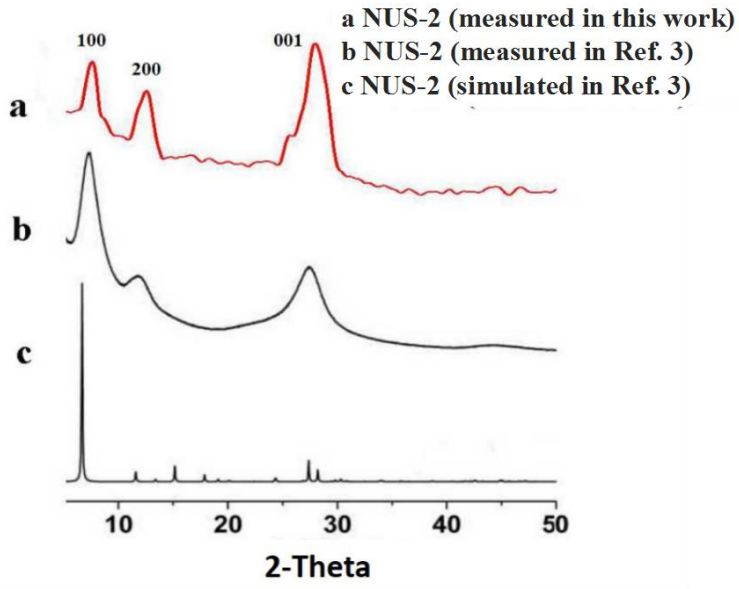

Fig. S15 The measured PXRD patterns of **NUS-2** (a), which were well consistent with the reported results (b and c). The peak at 6.9, 11.8, and 26.8° attributed to the (100), (200), and (001) reflection planes, respectively.

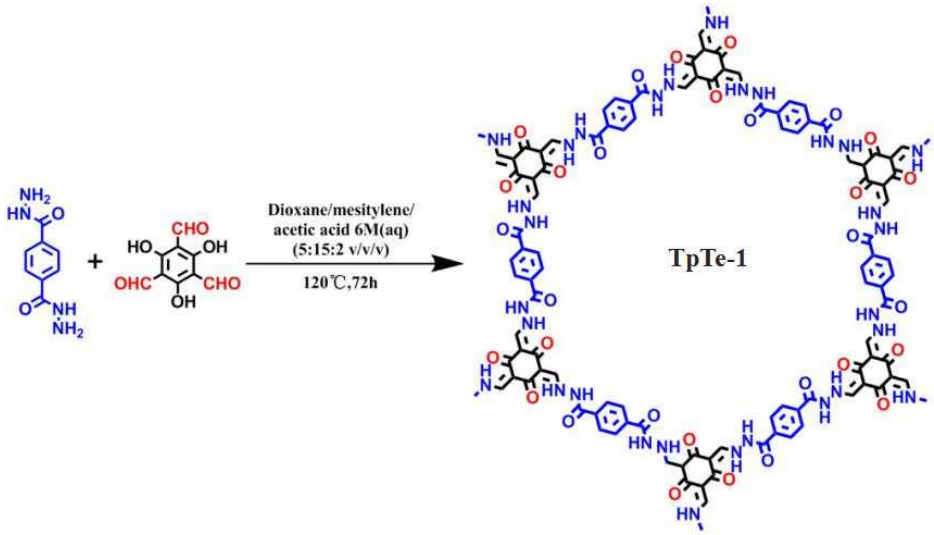

Scheme S6. Synthesis of **TpTe-1**.

Synthesis of TpTe-1. Terephthalohydrazide (0.15 mmol) and 1,3,5-triformylphloroglucinol (0.10 mmol, Tp) were weighed into a glass pressure tubing. After addition of 1,4-dioxane (1.0 mL), mesitylene (3.0 mL), and 0.4 mL of 6.0 M aqueous acetic acid, the tube was then flash frozen at 77 K (liquid N_2 bath) and degassed by three freeze-pump-thaw cycles. The tube was sealed off and then heated at 120 °C for 3 days. A yellow colored precipitate was isolated by centrifugation and washed with acetone (3×10 mL) and THF (3×10 mL), dried at 80 °C under vacuum for 24 h to yield **TpTe-1** as yellow powder in 80 % yield. Elemental analysis: cald for $(C_7H_5N_2O_2)_n$ (%): C 56.38, H

3.38, N 18.79; found: C 56.47, H 3.43, N 18.50. FTIR (KBr, cm^{-1}): 3200 (w), 2973 (w), 1628 (s), 1593 (s), 1325 (m), 1277 (s), 1187 (s), 1046 (m), 876 (m), 782 (m), 715 (m). Solid-state ^{13}C CP-MAS NMR (500 MHz, δ, ppm): 184, 147, 135, 130, 121, 115, 107, 101.

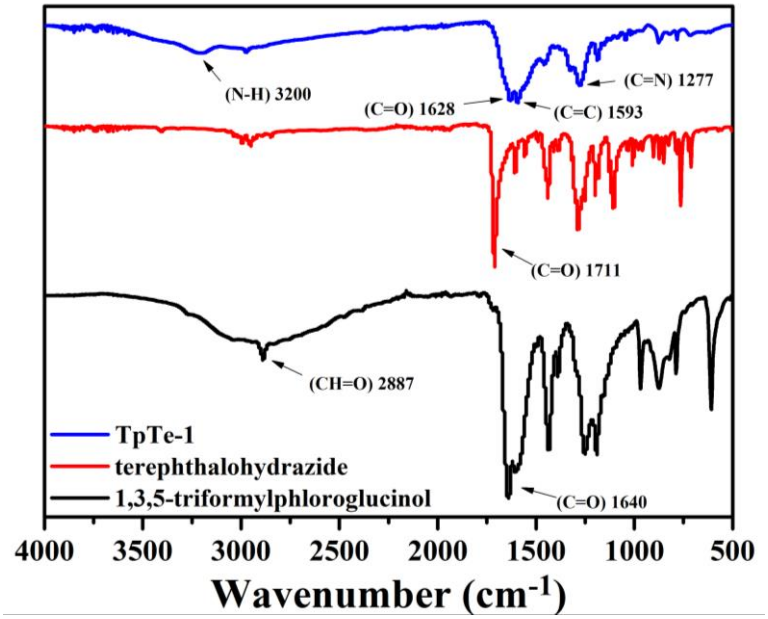

Fig. S16 IR spectra of **TpTe-1**, 1,3,5-triformylphloroglucinol, and terephthalohydrazide. The characteristic stretching vibration at 1640 cm^{-1} for the carbonyl stretching band of 1,3,5-trifornylphloroglucinol disappeared after the reaction. Meanwhile, a series of new characteristic stretching bands at 1628, 1593, and 1277 cm^{-1} for **TpTe-1** arising from the C=O, C=C, and C=N stretching bands, respectively, were observed indicating the successful condensation reaction.

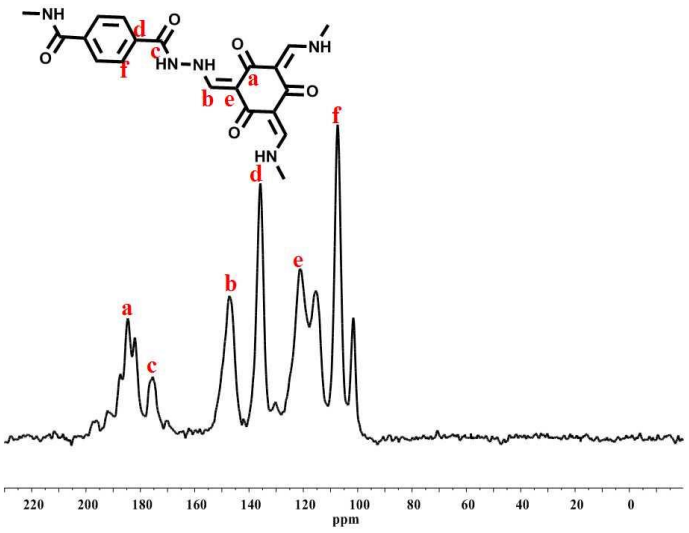

Fig. S17 Solid-state ^{13}C-MAS NMR spectrum of **TpTe-1**. The peak at 184 and 135 ppm could be

ascribed as the carbonyl carbon [*C*=O] of the keto form. The peak at 147 ppm confirms the presence of the *C*-N bond. The peaks at 130, 121, and 107 ppm belongs to the Ar groups interephthalohydrazide. The peak at 101 ppm correspond to the sp^2 hybridized olefinic carbon *C*=*C* groups.

Simulated structure of TpTe-1 (Molecular Modeling): Structural modeling of **TpTe-1** was performed by the Materials Studio (ver. 7.0) suite of programs. Molecular geometry optimization was conducted with MS DMol3 module. The initial lattice was created by starting with the space group *P*6/M. The *a* and *b* lattice parameters (initially 32.96 Å) were estimated according to the centre to centre distance between the vertices of the **TpTe-1**. The constructed model was geometry optimized using the Forcite module (Universal force fields, Ewald summations). Then the calculated PXRD pattern was generated with the Reflex Plus module. Finally, Pawley refinement was applied for profile fitting, producing the refined PXRD profile with the lattice parameters of *a* = *b* = 32.96 (± 0.002) Å and *c* = 3.50 (± 0.002) Å. *R*wp and *R*p values converged to 3.12% and 2.72%, respectively. A staggered arrangement for **TpTe-1** was also constructed with the space group P6/M wherein the stacked units were offset by a/2 and b/2. Comparison of the observed and the simulated PXRD patterns suggested that the preferable structure of **TpTe-1** is the eclipsed arrangement.

Table S1. Fractional atomic coordinates for the unit cell of the **TpTe-1** (AA stacking mode).

TpTe-1 AA stacking mode Space group: *P*6/M *a* = 32.96 Å, *b* = 32.96 Å, *c* = 3.50 Å *α* = 90.0°, *β* = 90.0°, *γ* = 120.0°			
Atom	x	y	z
C1	0.01298	-2.44816	0.49924
C2	-0.03885	-2.48702	0.49873
C3	-0.05182	-2.53885	0.50006
C4	0.10366	-2.42229	0.50012
O5	0.11645	-2.37144	0.49929
N6	-0.1417	-2.56493	0.49947
N7	0.19156	-2.39788	0.50011
C8	0.22952	-2.4108	0.49989
C9	0.28143	-2.37213	0.49975
C10	0.29475	-2.32018	0.49989
O11	0.25697	-2.30701	0.49988
H12	-0.06762	-2.47742	0.49737

H13	-0.1323	-2.52755	0.49885
H14	0.20106	-2.36047	0.49996
H15	0.21976	-2.44922	0.49983
H16	0.59162	0.56185	0.50076

Table S2. Fractional atomic coordinates for the unit cell of the **TpTe-1** (AB stacking mode).

TpTe-1 AB stacking mode Space group: *P*63/M *a* = 32.96 Å, *b* = 32.96 Å, *c* = 7.00 Å *α* = 90.0°, *β* = 90.0°, *γ* = 120.0°			
Atom	x	y	z
C1	0.34631	0.2185	0.25
C2	0.29448	0.17965	0.25
C3	0.28151	0.12782	0.25
C4	0.43699	0.24438	0.25
O5	0.44979	0.29522	0.25
N6	0.19163	0.10174	0.25
N7	0.52489	0.26878	0.25
C8	0.56285	0.25587	0.25
C9	0.61477	0.29453	0.25
C10	0.62809	0.34648	0.25
O11	0.5903	0.35966	0.25
C12	0.32036	0.11483	0.25
C13	0.37219	0.15368	0.25
C14	0.38515	0.20551	0.25
C15	0.22968	0.08895	0.25
O16	0.21688	0.03811	0.25
N17	0.47504	0.23159	0.25
N18	0.14178	0.06455	0.25
C19	0.10381	0.07746	0.25
C20	0.0519	0.0388	0.25
C21	0.03858	0.98685	0.25
O22	0.07636	0.97368	0.25
C23	0.7815	0.12781	0.25
C24	0.82035	0.11483	0.25
C25	0.87218	0.15369	0.25
C26	0.75562	0.19261	0.25
O27	0.70478	0.15456	0.25
N28	0.89826	0.08989	0.25
N29	0.73122	0.25611	0.25
C30	0.74413	0.30699	0.25
C31	0.70547	0.32023	0.25
C32	0.65352	0.2816	0.25
O33	0.64034	0.23065	0.25

C34	0.88517	0.20553	0.25
C35	0.84632	0.21851	0.25
C36	0.79449	0.17964	0.25
C37	0.91105	0.14072	0.25
O38	0.96189	0.17877	0.25
N39	0.76841	0.24344	0.25
N40	0.93545	0.07723	0.25
C41	0.92254	0.02635	0.25
C42	0.9612	0.0131	0.25
C43	0.01315	0.05173	0.25
O44	0.02632	0.10269	0.25
C45	0.87219	0.65369	0.25
C46	0.88517	0.70552	0.25
C47	0.84631	0.71849	0.25
C48	0.80739	0.56301	0.25
O49	0.84544	0.55021	0.25
N50	0.91011	0.80837	0.25
N51	0.74389	0.47511	0.25
C52	0.69301	0.43715	0.25
C53	0.67977	0.38523	0.25
C54	0.7184	0.37191	0.25
O55	0.76935	0.4097	0.25
C56	0.79447	0.67964	0.25
C57	0.78149	0.62781	0.25
C58	0.82036	0.61485	0.25
C59	0.85928	0.77032	0.25
O60	0.82123	0.78312	0.25
N61	0.75656	0.52496	0.25
N62	0.92277	0.85822	0.25
C63	0.97365	0.89619	0.25
C64	0.9869	0.9481	0.25
C65	0.94827	0.96142	0.25
O66	0.89731	0.92364	0.25
C67	0.65369	0.7815	0.75
C68	0.70552	0.82035	0.75
C69	0.71849	0.87218	0.75
C70	0.56301	0.75562	0.75
O71	0.55021	0.70478	0.75
N72	0.80837	0.89826	0.75
N73	0.47511	0.73122	0.75
C74	0.43715	0.74413	0.75
C75	0.38523	0.70547	0.75
C76	0.37191	0.65352	0.75

O77	0.4097	0.64034	0.75
C78	0.67964	0.88517	0.75
C79	0.62781	0.84632	0.75
C80	0.61485	0.79449	0.75
C81	0.77032	0.91105	0.75
O82	0.78312	0.96189	0.75
N83	0.52496	0.76841	0.75
N84	0.85822	0.93545	0.75
C85	0.89619	0.92254	0.75
C86	0.9481	0.9612	0.75
C87	0.96142	0.01315	0.75
O88	0.92364	0.02632	0.75
C89	0.2185	0.87219	0.75
C90	0.17965	0.88517	0.75
C91	0.12782	0.84631	0.75
C92	0.24438	0.80739	0.75
O93	0.29522	0.84544	0.75
N94	0.10174	0.91011	0.75
N95	0.26878	0.74389	0.75
C96	0.25587	0.69301	0.75
C97	0.29453	0.67977	0.75
C98	0.34648	0.7184	0.75
O99	0.35966	0.76935	0.75
C100	0.11483	0.79447	0.75
C101	0.15368	0.78149	0.75
C102	0.20551	0.82036	0.75
C103	0.08895	0.85928	0.75
O104	0.03811	0.82123	0.75
N105	0.23159	0.75656	0.75
N106	0.06455	0.92277	0.75
C107	0.07746	0.97365	0.75
C108	0.0388	0.9869	0.75
C109	0.98685	0.94827	0.75
O110	0.97368	0.89731	0.75
C111	0.12781	0.34631	0.75
C112	0.11483	0.29448	0.75
C113	0.15369	0.28151	0.75
C114	0.19261	0.43699	0.75
O115	0.15456	0.44979	0.75
N116	0.08989	0.19163	0.75
N117	0.25611	0.52489	0.75
C118	0.30699	0.56285	0.75
C119	0.32023	0.61477	0.75

C120	0.2816	0.62809	0.75
O121	0.23065	0.5903	0.75
C122	0.20553	0.32036	0.75
C123	0.21851	0.37219	0.75
C124	0.17964	0.38515	0.75
C125	0.14072	0.22968	0.75
O126	0.17877	0.21688	0.75
N127	0.24344	0.47504	0.75
N128	0.07723	0.14178	0.75
C129	0.02635	0.10381	0.75
C130	0.0131	0.0519	0.75
C131	0.05173	0.03858	0.75
O132	0.10269	0.07636	0.75
H133	0.35592	0.25688	0.25
H134	0.20103	0.13912	0.25
H135	0.53439	0.30619	0.25
H136	0.5531	0.21745	0.25
H137	0.31074	0.07645	0.25
H138	0.46564	0.19421	0.25
H139	0.13228	0.02714	0.25
H140	0.11356	0.11588	0.25
H141	0.74312	0.09904	0.25
H142	0.86088	0.06192	0.25
H143	0.69381	0.22821	0.25
H144	0.78255	0.33566	0.25
H145	0.92355	0.23429	0.25
H146	0.80579	0.27141	0.25
H147	0.97286	0.10514	0.25
H148	0.88412	-0.00232	0.25
H149	0.90096	0.64408	0.25
H150	0.93809	0.79897	0.25
H151	0.77179	0.4656	0.25
H152	0.66435	0.44691	0.25
H153	0.76571	0.68926	0.25
H154	0.72858	0.53436	0.25
H155	0.89486	0.86772	0.25
H156	1.00232	0.88644	0.25
H157	0.64408	0.74312	0.75
H158	0.79897	0.86088	0.75
H159	0.46561	0.69381	0.75
H160	0.4469	0.78255	0.75
H161	0.68926	0.92355	0.75
H162	0.53436	0.80579	0.75

H163	0.86772	0.97286	0.75
H164	0.88644	0.88412	0.75
H165	0.25688	0.90096	0.75
H166	0.13912	0.93808	0.75
H167	0.30619	0.77179	0.75
H168	0.21745	0.66434	0.75
H169	0.07645	0.76571	0.75
H170	0.19421	0.72859	0.75
H171	0.02714	0.89486	0.75
H172	0.11588	1.00232	0.75
H173	0.09904	0.35592	0.75
H174	0.15369	0.28151	0.59167
H175	0.06191	0.20103	0.75
H176	0.22821	0.5344	0.75
H177	0.33565	0.55309	0.75
H178	0.23429	0.31074	0.75
H179	0.27142	0.46564	0.75
H180	0.10514	0.13228	0.75
H181	-0.00232	0.11356	0.75
H182	0.26571	0.18926	0.25
H183	0.28151	0.12782	0.09167
H184	0.40096	0.14407	0.25
H185	0.81074	0.07645	0.25
H186	0.85593	0.25689	0.25
H187	0.79449	0.17964	0.09167
H188	0.92355	0.73429	0.25
H189	0.84631	0.71849	0.09167
H190	0.74311	0.59904	0.25
H191	0.82036	0.61485	0.09167
H192	0.73429	0.81074	0.75
H193	0.71849	0.87218	0.59167
H194	0.59904	0.85593	0.75
H195	0.61485	0.79449	0.59167
H196	0.18926	0.92355	0.75
H197	0.12782	0.84631	0.59167
H198	0.14407	0.74311	0.75
H199	0.20551	0.82036	0.59167
H200	0.07645	0.26571	0.75
H201	0.25689	0.40096	0.75
H202	0.17964	0.38515	0.59167

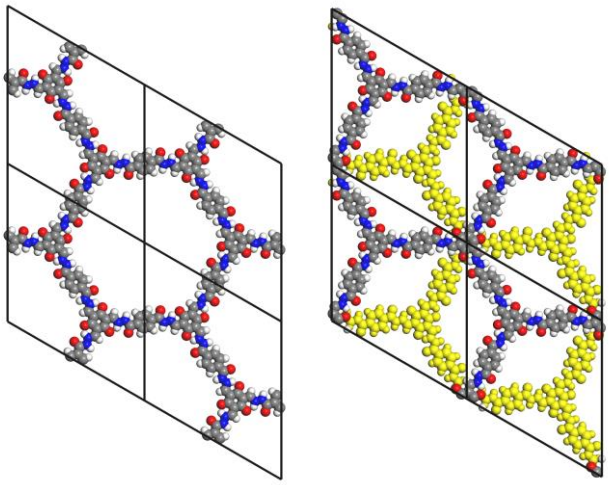

Fig. S18 Left: AA-type staggered structure of **TpTe-1**. Right: AB-type staggered structure of **TpTe-1**. Compared to AB-type staggered structure, the eclipsed model is more energetic preferential depending on the force-field-based molecular mechanics calculations.

Synthesis of Pd@TpTe-1. TpTe-1 (100 mg) was added to a CH_3OH (20 mL) solution of palladium nitrate (67 mg, 0.29 mmol). The mixture was stirred for 1 h at room temperature. The resulting solid was isolated by centrifugation and washed with CH_3CN. The obtained green-yellow crystalline solid was mixed with $NaBH_4$ (80 mg, 2.11 mmol) in 20 mL of water, and the mixture was stirred at room temperature for an additional 5 h to afford Pd@COF as dark brown crystalline solids. The obtained crystalline solids were washed with CH_3CN and EtOH and dried under vacuum. ICP measurement indicated that the encapsulated amount of Pd NPs in the **Pd@TpTe-1** is 6.8 wt%.

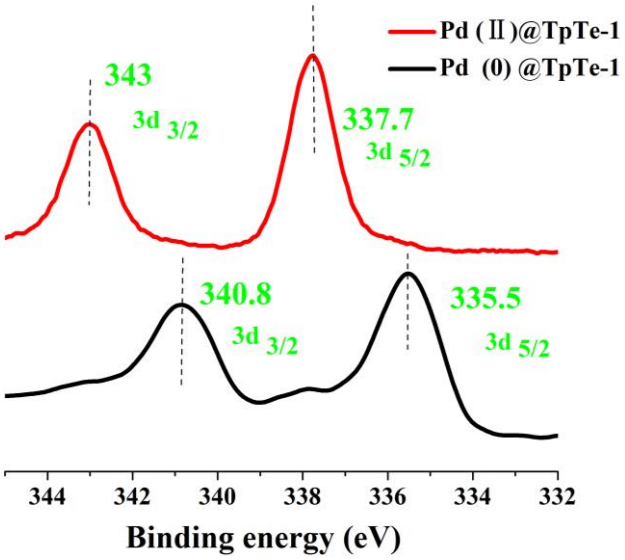

Fig. S19 XPS spectra of **Pd@TpTe-1** for oxidation state of the encapsulated Pd species before

and after reduction.

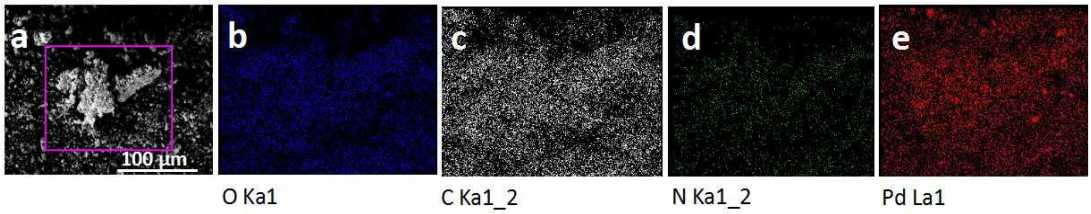

Fig. S20 SEM-EDX elemental mapping of **Pd@TpTe-1**.

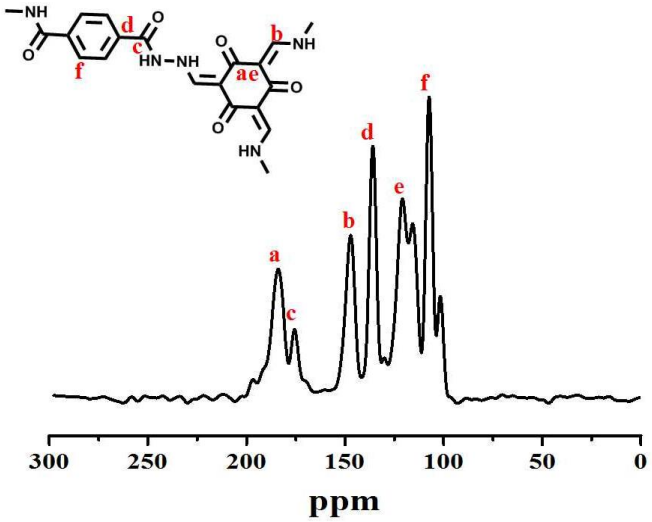

Fig. S21 Solid-state ^{13}C-MAS spectrum of **Pd@TpTe-1**. Compared to **TpTe-1**, no difference was observed, indicating the **TpTe-1** framework was stable during the Pd(II) reducing process. [4]

3. Fabrication and characterization of COF-based aerogels

Characterization of chitosan-aerogel based on amino-epoxy reaction.

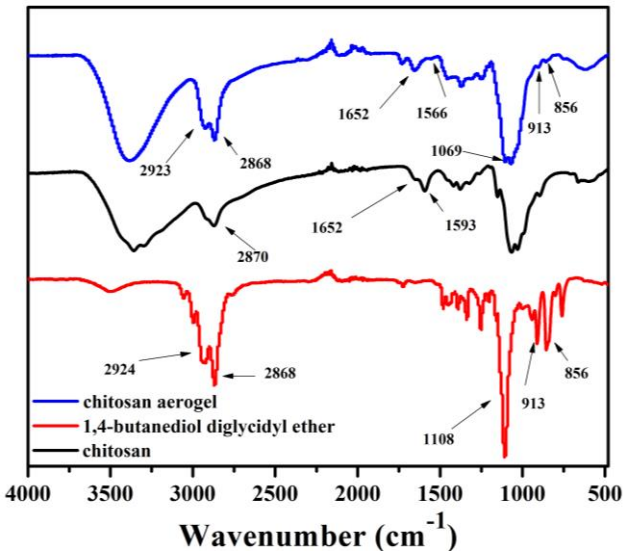

Fig. S22 IR spectra of chitosan (95% degree of deacetylation), 1,4-butanediol diglycidyl ether and chitosan-aerogel. As indicated in Fig. S22, the characteristic peaks at 856 and 913 cm^{-1} attributed

to epoxy group basically disappeared in the spectrum of chitosan-aerogel. However, the peaks at 2924 and 2868 cm^{-1} corresponding to methylene bands and the peak at 1108 cm^{-1} for C-O-C band were still present in the spectrum of chitosan-aerogel. In addition, the band at 1593 cm^{-1} that corresponds to the primary amine group on chitosan was shifted to 1566 cm^{-1}, and the peak area was significantly decreased in the spectrum for chitosan-aerogel. Thus, the FTIR analysis confirmed the successful conjugation of 1,4-butanediol diglycidyl ether to the amine group of chitosan. The peak at 1652 cm^{-1} corresponds to the residual amide moiety of commercial chitosan.

Fabrication of COF-based hybrid aerogels. In a typical synthesis, 0.2 g of chitosan powder was dissolved in 20 mL of deionized water added with 120 μL of acetic acid with stirring, until a transparent solution formed. Then 0.2 g of COF powder was added into the chitosan solution. Following strong stirring and ultrasonic shaking, 480 μL of 1,4-Butanediol diglycidyl ether was added as the cross-linker. Then, the composite solution was immediately transferred into mold. The mold containing the solution was stand for ca. 10 h until a stable hydrogel was formed. Then, the obtained hydrogel was slowly transferred into a cooler for 12 h to generate the ice crystals. Finally, the frozen sample was freeze-dried at minus 50 °C for approximately 24 h in a freeze-dryer to form the dry COF-chitosan aerogel with 50 wt% of COF loading. The synthetic procedure was in a similar way for other types of COF-based aerogel monoliths.

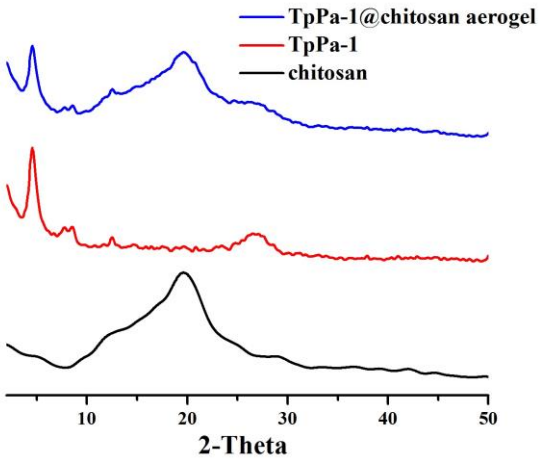

Fig. S23 PXRD patterns of chitosan, **TpPa-1**, and **TpPa-1@chitosan** aerogel. The structural integrity and crystallinity of **TpPa-1** were well retained during the processing process (see the 2θ value at 4.5°). In addition, the chitosan species (2θ value at 20.3°) were also detected in **TpPa-1@chitosan** aerogel.

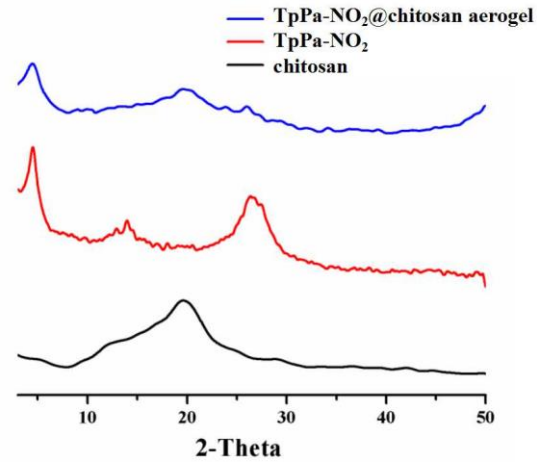

Fig. S24 PXRD patterns of chitosan, **TpPa-NO$_2$**, and **TpPa-NO$_2$@chitosan** aerogel. The structural integrity and crystallinity of **TpPa-NO$_2$** were well retained during the processing process (see the 2θ value at 4.5^o). In addition, the chitosan species (2θ value at 20.3^o) were also detected in **TpPa-1@chitosan** aerogel.

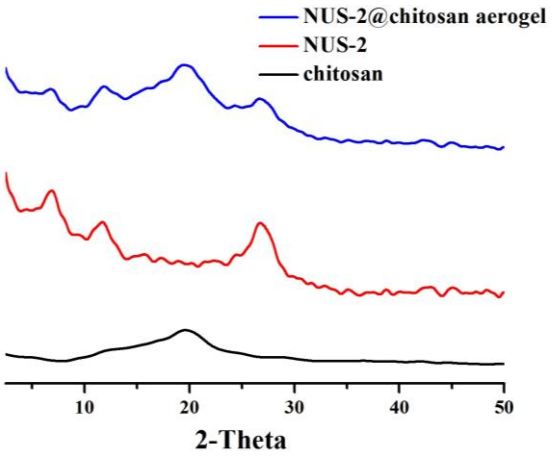

Fig. S25 PXRD patterns of chitosan, **NUS-2**, and **NUS-2@chitosan** aerogel. The structural integrity and crystallinity of **NUS-2** were well retained during the processing process (see the 2θ value at 6.9^o). In addition, the chitosan species (2θ value at 20.3^o) were also detected in **NUS-2@chitosan** aerogel.

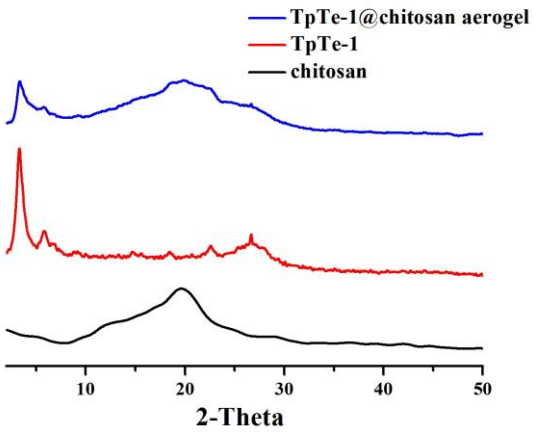

Fig. S26 PXRD patterns of chitosan, **TpTe-1**, and **TpTe-1@chitosan** aerogel. The structural integrity and crystallinity of **TpTe-1** were well retained during the processing process (see the 2θ value at 3.3º). In addition, the chitosan species (2θ value at 20.3º) were also detected in **TpTe-1@chitosan** aerogel.

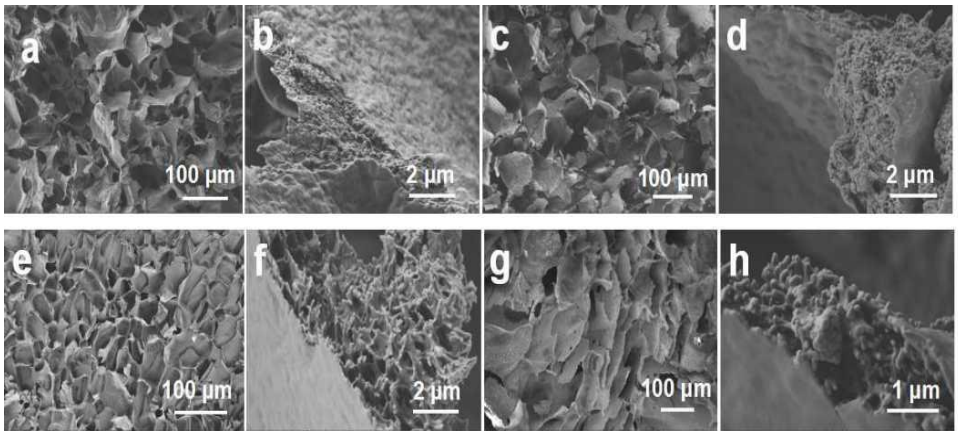

Fig. S27 SEM image of **TpPa-1@chitosan** aerogel (a, b), **TpPa-NO$_2$@chitosan** aerogel (c, d), **NUS-2@chitosan** aerogel (e, f), and **TpTe-1@chitosan** aerogel (g, h).

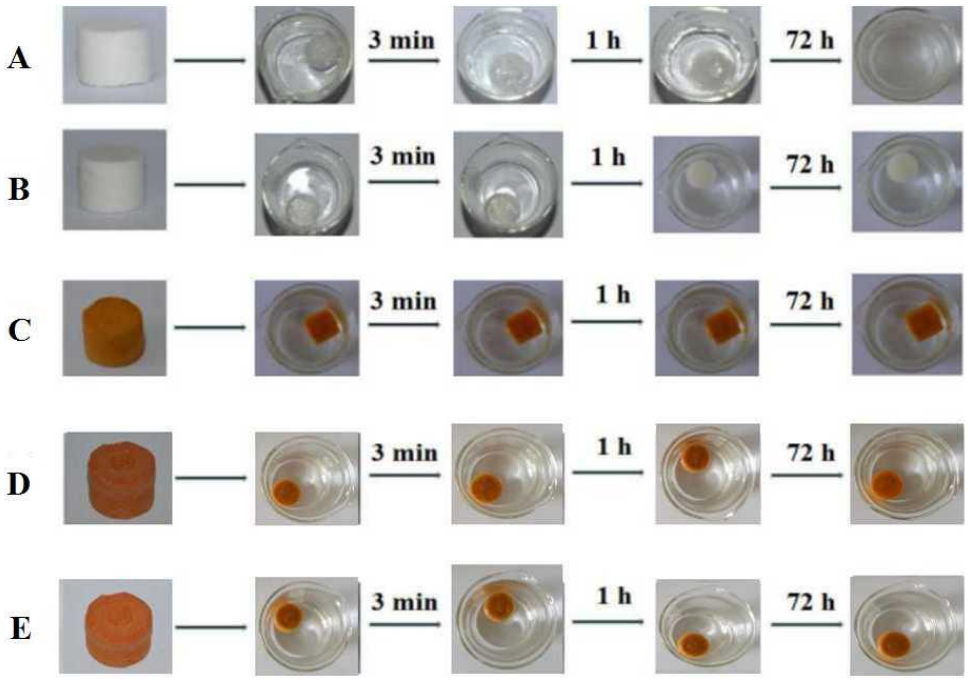

Fig. S28 The stability tests for pure chitosan aerogel (A), cross-linked chitosan aerogel (B), and hybrid **TpTe-1@chitosan** aerogel in (C) water, (D) ethanol, and (E) acetone. As indicated in A, the pure chitosan without cross-linker of 1,4-butanediol diglycidyl ether is not stable in water. In contrast, the cross-linker involved aerogels (B-E) are very stable in water, ethanol and acetone.

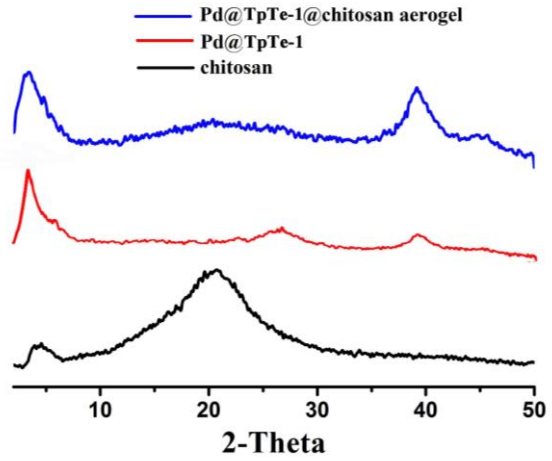

Fig. S29 PXRD patterns of chitosan, **Pd@TpTe-1**, and **Pd@TpTe-1@chitosan** aerogel.

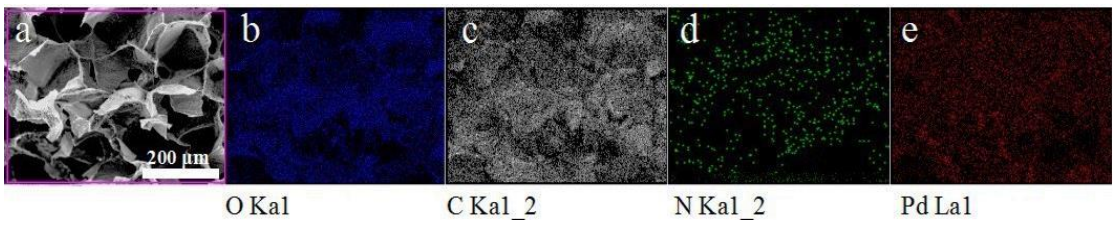

Fig. S30 SEM-EDX elemental mapping of **Pd@TpTe-1@chitosan** aerogel.

Fig. S31 The photo images of **Pd@TpTe-1@chitosan** aerogel. Top: cylindric hybrid aerogel monoliths, Bottom: tubular cylindric hybrid aerogel casting.

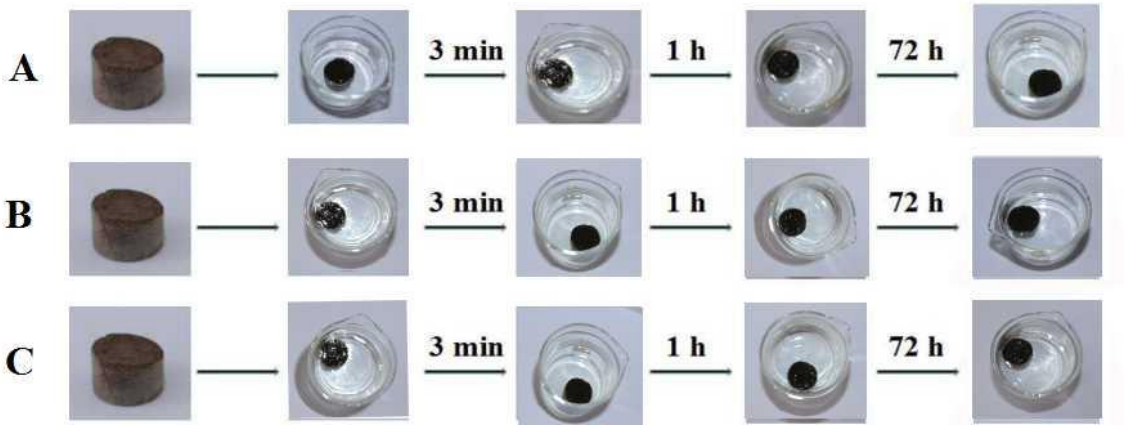

Fig. S32 The stability tests for the hybrid **Pd@TpTe-1@chitosan** aerogel in water (A), ethanol (B), and acetone (C). It showed that the hybrid **Pd@TpTe-1@chitosan** aerogel is very stable in water, ethanol, and acetone.

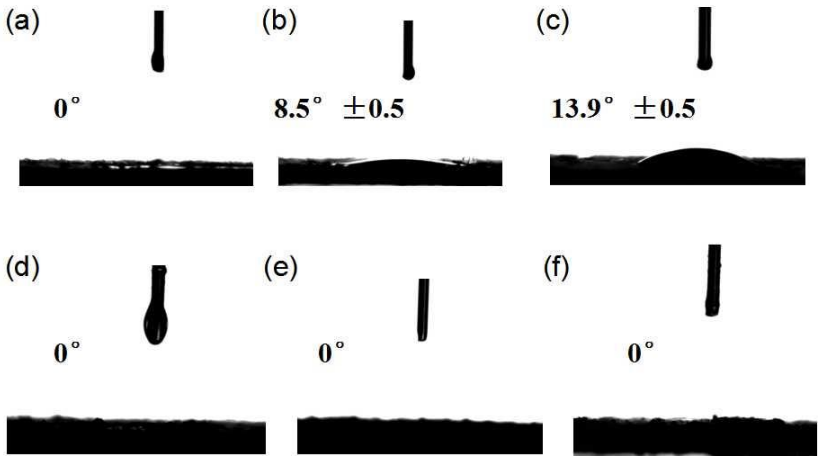

Fig. S33 Contact angles of the samples: (a) chitosan powder, (b) **TpTe-1**, (c) **Pd@TpTe-1**, (d) chitosan aerogel, (e) **TpTe-1@chitosan** aerogel, (f) **Pd@TpTe-1@chitosan** aerogel.

Table S3. The water uptake and dimensional stability of the samples.

Sample	Water uptake (wt%)	Swelling rate (%)
TpTe-1	735	—
Pd@TpTe-1	536	—
chitosan aerogel	2294	5.6
TpTe-1@chitosan aerogel	1876	3.1
Pd@TpTe-1@chitosan aerogel	1319	2.9

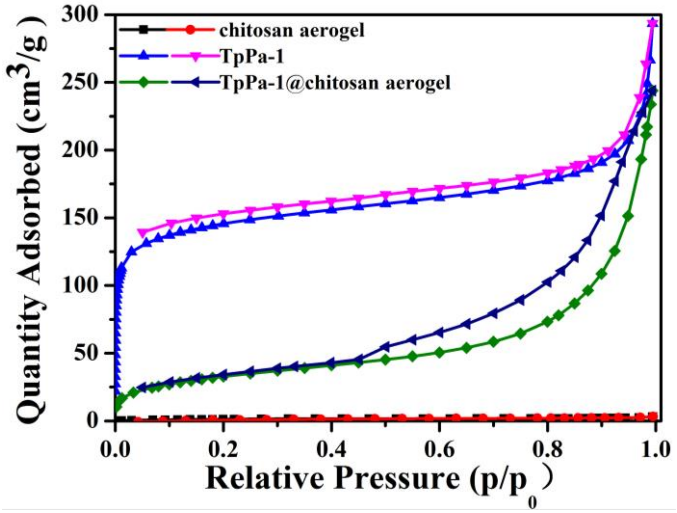

Fig. S34 N_2 sorption isotherms of pure chitosan aerogel, **TpPa-1**, and **TpPa-1@chitosan**.

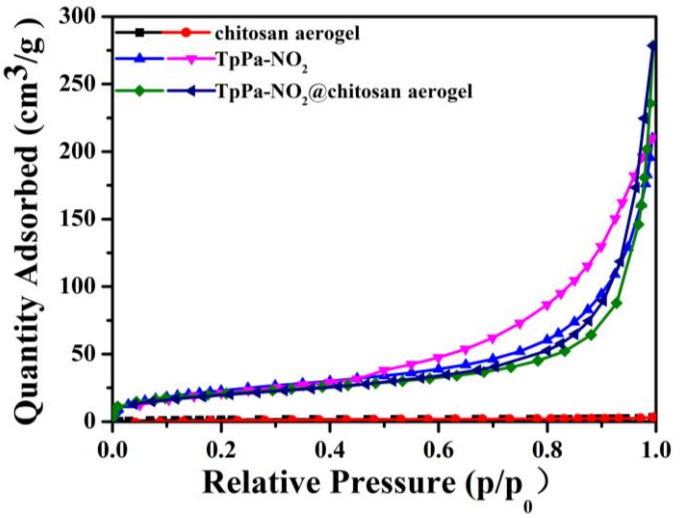

Fig. S35 N_2 sorption isotherms of pure chitosan aerogel, **TpPa-NO_2**, and **TpPa-NO_2 @chitosan**.

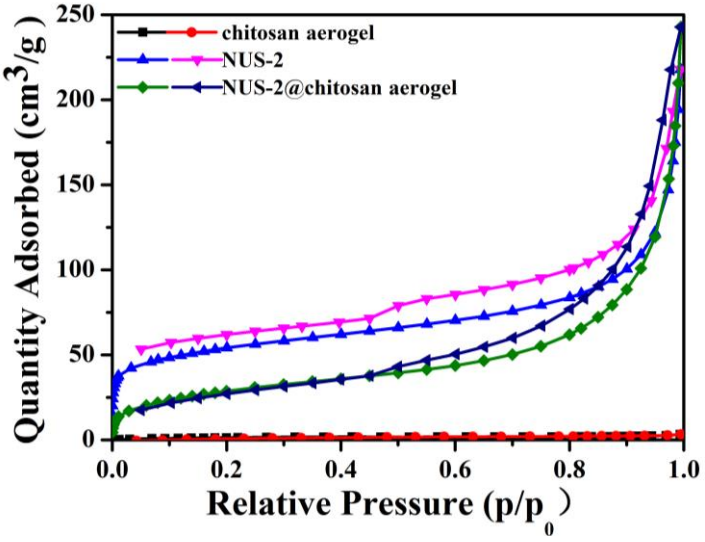

Fig. S36 N_2 sorption isotherms of pure chitosan aerogel, **NUS-2**, and **NUS-2@chitosan**.

Table S4. The BET surface areas, nitrogen adsorption quantities for pure chitosan, COFs, Pd@COF and the hybrid aerogels based on measured N_2 sorption isotherms.

Sample	BET Surface Area (m^2/g)	Adsorption quantity (cm^3/g)
TpPa-1	499.9	293.6
TpPa-NO_2	268.1	432.1
NUS-2	175.0	162.1
TpTe-1	359.6	249.8
Pd@TpTe-1	107.3	189.9
chitosan aerogel	5.6	3.2
TpPa-1@chitosan aerogel	121.9	243.0
TpPa-NO_2@chitosan aerogel	87.9	209.9
NUS-2@chitosan aerogel	107.7	242.8
TpTe-1@chitosan aerogel	83.4	217.4
Pd@TpTe-1@chitosan aerogel	55.7	161.4

4. General procedure for the Pd@TpTe-1-catalyzed dechlorinating reaction

Batch experiment. A mixture of ArCl (0.5 mmol), HCO_2NH_4 (5 mmol) and **Pd@TpTe-1** (25 mg, 3.0 mol % of Pd) in water (5 mL) was stirred at room temperature (Yield was determined by GC analysis).

Catalyst recovery. After each run, the catalyst was collected by centrifugation, washed with ethanol and air dried for next catalytic run under the same conditions. Solid catalyst of **Pd@TpTe-1** could be reused for at least five catalytic runs for the model reaction.

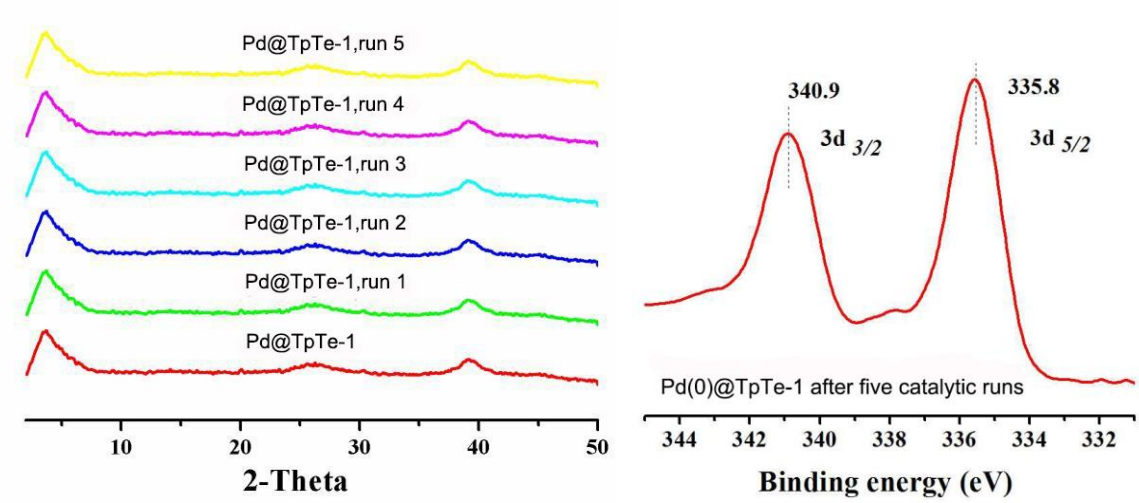

Fig. S37 Left: PXRD patterns of **Pd@TpTe-1** and it after five catalytic runs. Right: XPS spectrum of Pd species in **Pd@TpTe-1** after five catalytic runs. No COF structural and Pd valence changes were detected after catalytic runs.

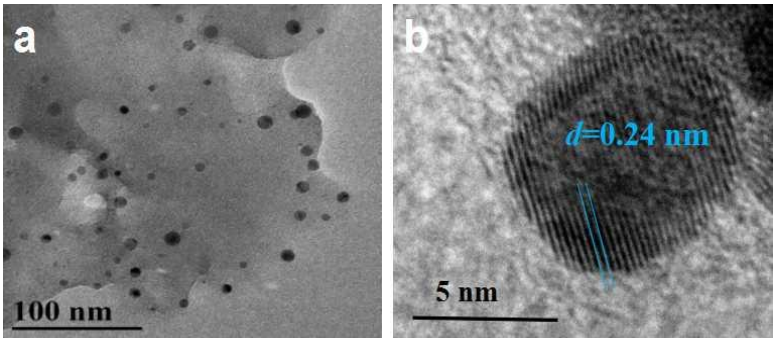

Fig. S38 HRTEM images of **Pd@TpTe-1** after five catalytic runs.

Table S5. ICP result for **Pd@TpTe-1** before and after five catalytic runs.

Sample	**Pd@TpTe-1**	
	before	after
Pd wt %	6.80	6.78

5. Continuous flow-through operation

The aqueous solution (10 mL) of *p*-chlorophenol (1.0 mmol) and HCO_2NH_4 (10 mmol) was pumped through **Pd@TpTe-1@aerogel** flow-through microreactor (3 mol % Pd per piece) using a peristaltic pump with a flow rate of 1.0 mL min^{-1}. The reaction was monitored by GC analysis. For the amplified experiment, the aqueous (25 mL) solution of three-component CBs (*p*-chlorophenol, 1 mmol; *p*-chlorbenzoic acid, 1 mmol; *p*-chloroacetophenone, 1 mmol) and HCO_2NH_4 (30 mmol) was pumped through the COF-based aerogel-connected flow-through microreactor (1 mol % Pd per piece) by peristaltic pump with a flow rate of 1.0 mL min^{-1}. The reaction was monitored by GC

analysis.

For comparison, the Pd@chitosan aerogel was simply prepared by the reduction (250 mg $NaBH_4$, 10 mL H_2O, 5 h, r.t.) of Pd(II)@chitosan that was obtained by impregnating of chitosan aerogel (100 mg) in a solution of $Pd(NO_3)$ in MeOH (67 mg, 20 mL) at room temperature for 2 h. The resulting aerogel was washed with ethanol. The formation of Pd@chitosan was accompanied by a distinct visual colour change from white to dark. The loading amount of Pd NPs, as determined by inductively coupled plasma (ICP) measurement, is up to 4.98 wt %. The catalytic performance was carried out in the same condition with that of Pd@TpTe-1@chitosan aerogel: An aqueous solution (10 mL) of *p*-chlorophenol (1 mmol) and HCO_2NH_4 (10 mmol) was pumped through a piece of Pd@chitonsan aerogel monolith (64 mg, 3.0 mol % Pd) using a peristaltic pump at a flow rate of 1.0 mL/min. The reaction was monitored by GC analysis.

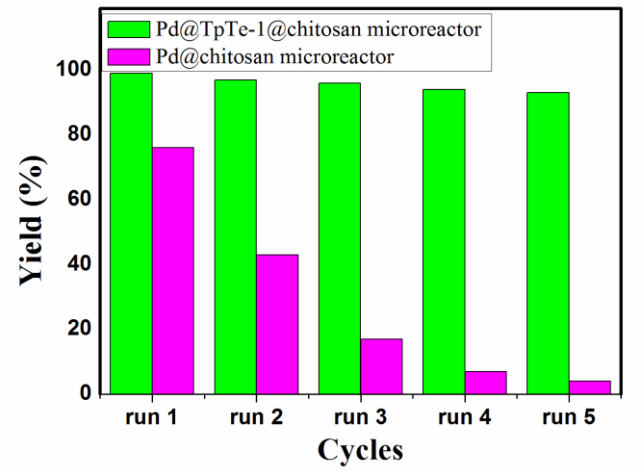

Fig. S39 Catalytic cycles for the *p*-chlorophenol dechlorination via **Pd@TpTe-1@chitosan** and **Pd@chitosan** flow-through microreactor. Reaction conditions: *p*-chlorophenol (1 mmol), HCO_2NH_4 (10 mmol), aerogel (3.0 mol % Pd), H_2O (10 mL), r.t., in air, Yield was determined by GC analysis. The **Pd@TpTe-1@chitosan** aerogel still showed excellent activity and the catalytic yield was even up to 93 % after five catalytic runs. However, the corresponding catalytic yield of **Pd@chitosan** went through a dramatic decreasing process from initial 76 % to 3.5 % after five catalytic runs.

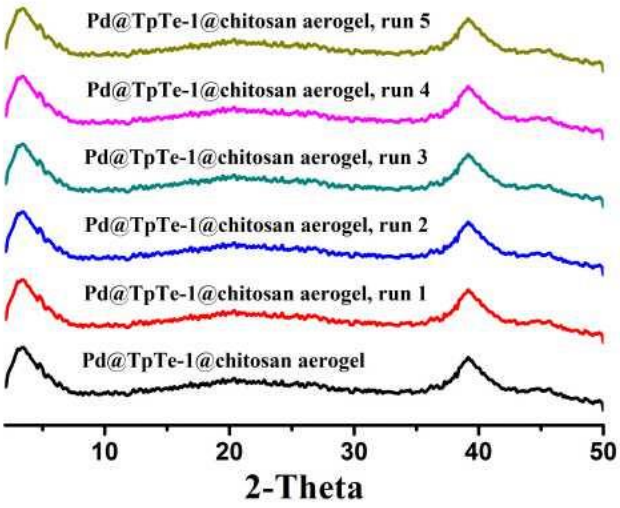

Fig. S40 PXRD patterns of **Pd@TpTe-1@chitosan** microreactor and it after five catalytic runs.

Table S6. ICP results before and after the continuous flow-through catalytic process for *p*-chlorophenol dechlorination.

Sample	**Pd@TpTe-1@chitosan** microreactor		Pd@chitosan microreactor	
	before	after	before	after
Pd wt %	3.50	3.48	4.98	2.32

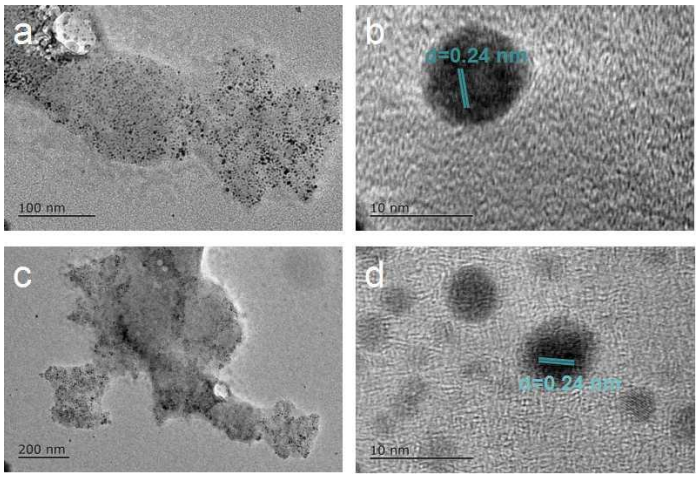

Fig. S41 HRTEM images of **Pd@TpTe-1@chitosan** microreactor before (a, b) and after (c, d) five catalytic runs.

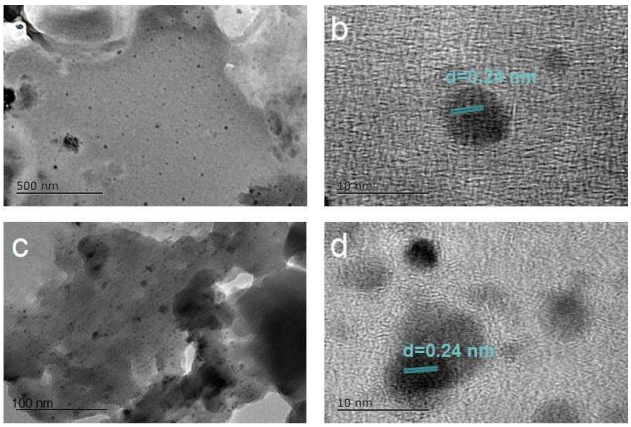

Fig. S42 HRTEM images of **Pd@chitosan** microreactor before (a, b) and after (c, d) five catalytic runs. Serious aggregation of Pd NPs after the catalytic runs was observed herein.

6. GC analysis for the aqueous CBs dechlorination in batch and continuous-flow microreactor experiments

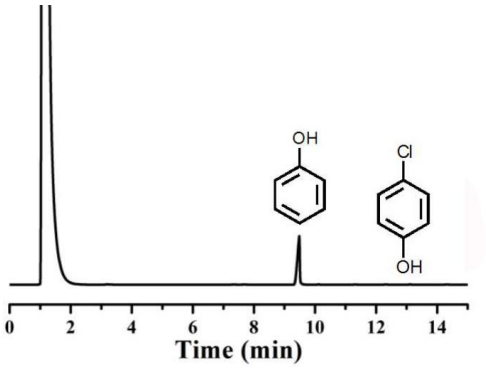

Fig. S43 GC analysis for the dechlorinating reaction of *p*-chlorophenol catalyzed by **Pd@TpTe-1** within 1.5 h in the batch experiment for the first run. The yield is 99 %.

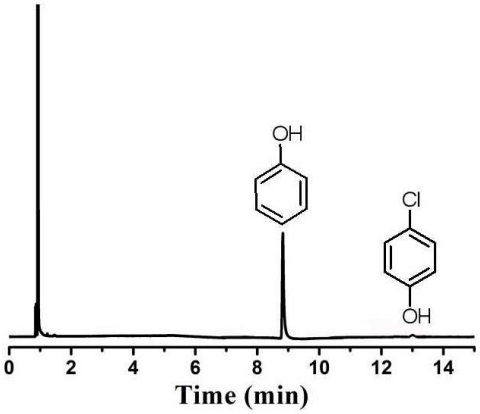

Fig. S44 GC analysis for the dechlorinating reaction of *p*-chlorophenol catalyzed by **Pd@TpTe-1** within 1.5 h in the batch experiment for the second run. The yield is 98 %.

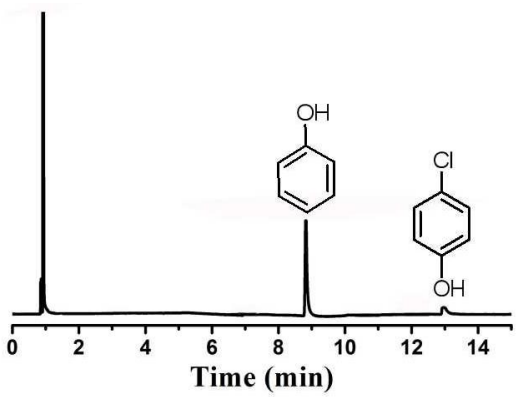

Fig. S45 GC analysis for the dechlorinating reaction of *p*-chlorophenol catalyzed by **Pd@TpTe-1** within 1.5 h in the batch experiment for the third run. The yield is 96 %.

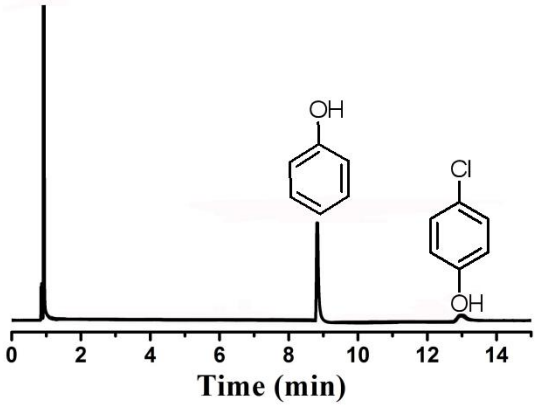

Fig. S46 GC analysis for the dechlorinating reaction of *p*-chlorophenol catalyzed by **Pd@TpTe-1** within 1.5 h in the batch experiment for the fourth run. The yield is 94 %.

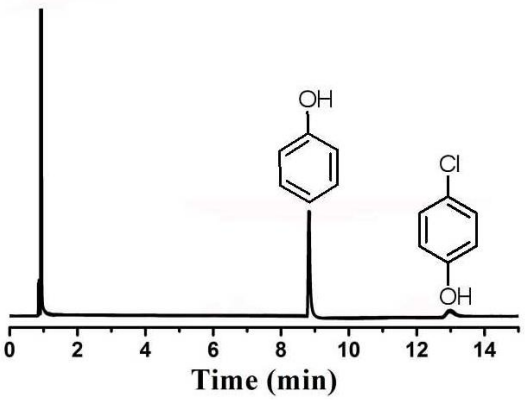

Fig. S47 GC analysis for the dechlorinating reaction of *p*-chlorophenol catalyzed by **Pd@TpTe-1** within 1.5 h in the batch experiment for the fifth run. The yield is 93.6 %.

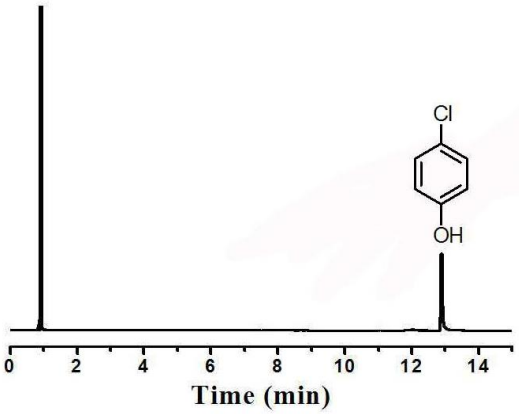

Fig. S48 GC analysis for the dechlorinating reaction of *p*-chlorophenol catalyzed by **TpTe-1** within 1.5 h in the batch experiment. The yield is 0 %.

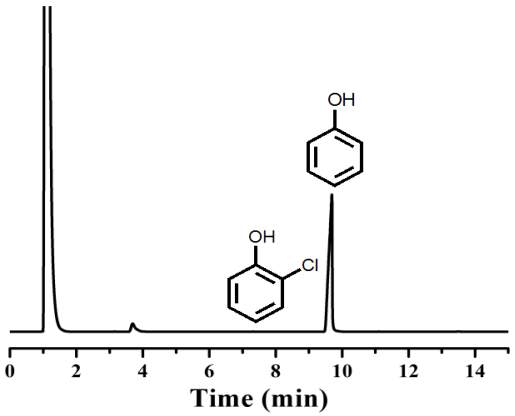

Fig. S49 GC analysis for the dechlorinating reaction of *o*-chlorophenol catalyzed by **Pd@TpTe-1** within 1.5 h in the batch experiment. The yield is 98 %.

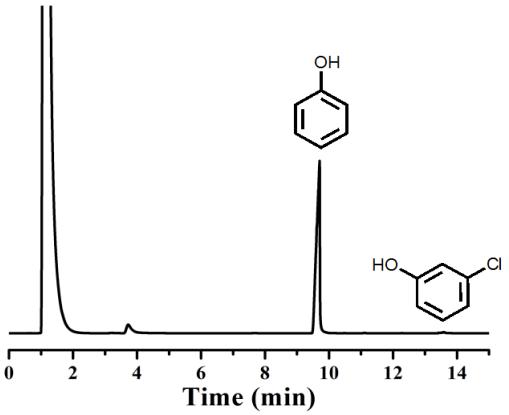

Fig. S50 GC analysis for the dechlorinating reaction of *m*-chlorophenol catalyzed by **Pd@TpTe-1** within 1.5 h in the batch experiment. The yield is 98%.

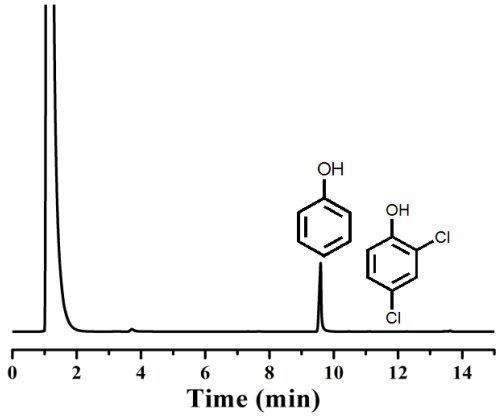

Fig. S51 GC analysis for the dechlorinating reaction of 2,4-dichlorophenol catalyzed by **Pd@TpTe-1** within 1.5 h in the batch experiment. The yield is 98%.

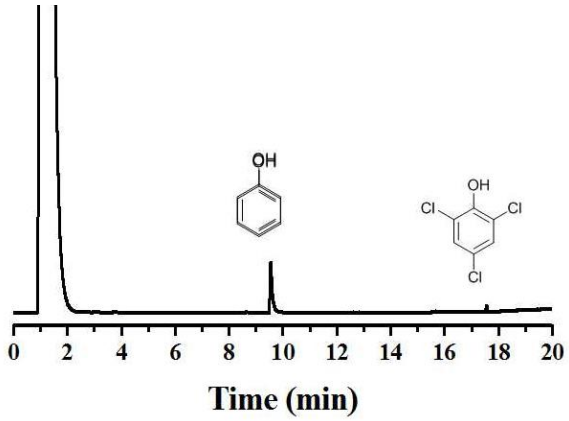

Fig. S52 GC analysis for the dechlorinating reaction of 2,4,6-trichlorophenol catalyzed by **Pd@TpTe-1** within 1.5 h in the batch experiment. The yield is 97%.

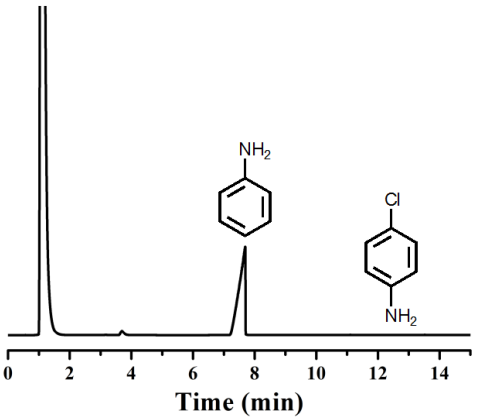

Fig. S53 GC analysis for the dechlorinating reaction of *p*-chloroaniline catalyzed by **Pd@TpTe-1** within 1.5 h in the batch experiment. The yield is 96%.

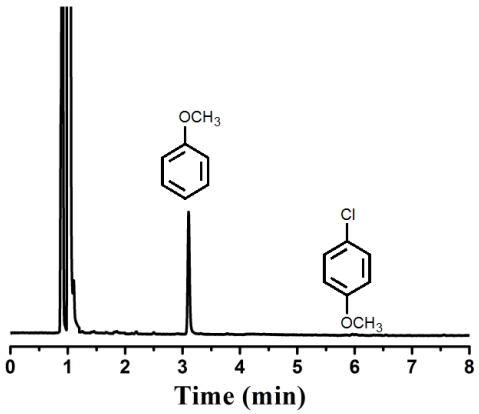

Fig. S54 GC analysis for the dechlorinating reaction of *p*-chloroanisole catalyzed by **Pd@TpTe-1** within 3 h in the batch experiment. The yield is 98%.

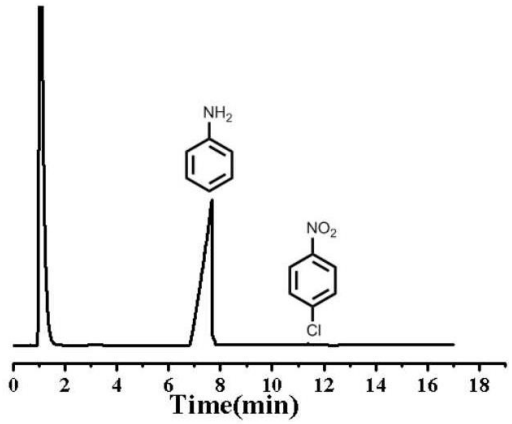

Fig. S55 GC analysis for the dechlorinating reaction of *p*-nitrchlorobenzene catalyzed by **Pd@TpTe-1** within 3 h in the batch experiment. The yield is ≥99%.

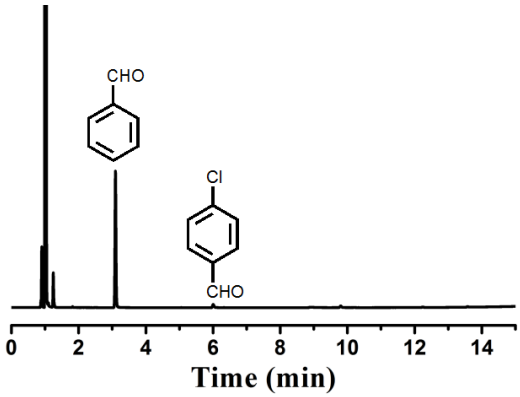

Fig. S56 GC analysis for the dechlorinating reaction of *p*-chlorobenzaldehyde catalyzed by **Pd@TpTe-1** within 6 h in the batch experiment. The yield is 98%.

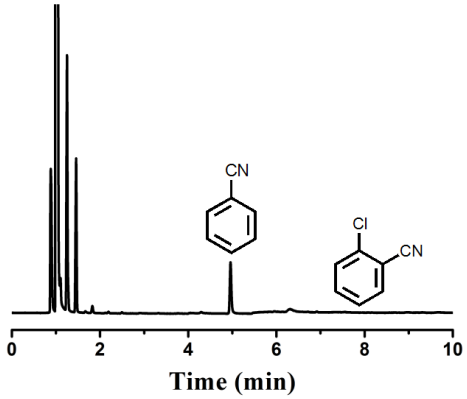

Fig. S57 GC analysis for the dechlorinating reaction of *o*-chlorobenzonitrile catalyzed by **Pd@TpTe-1** within 6 h in the batch experiment. The yield is ≥99%.

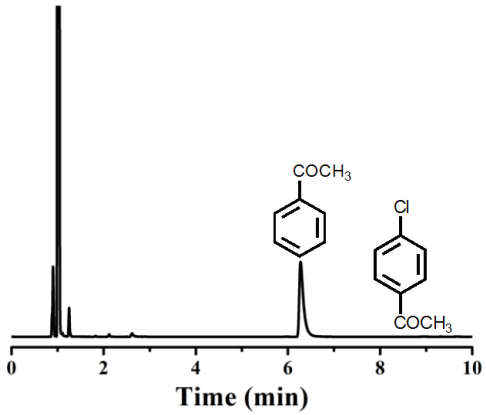

Fig. S58 GC analysis for the dechlorinating reaction of *p*-chloroacetophenone catalyzed by **Pd@TpTe-1** within 6 h in the batch experiment. The yield is ≥99%.

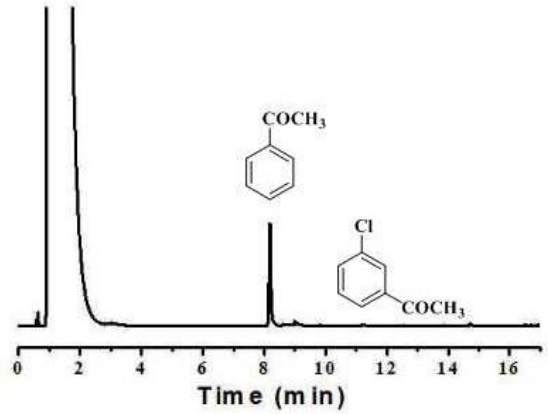

Fig. S59 GC analysis for the dechlorinating reaction of *m*-chloroacetophenone catalyzed by **Pd@TpTe-1** within 6 h in the batch experiment. The yield is 94%.

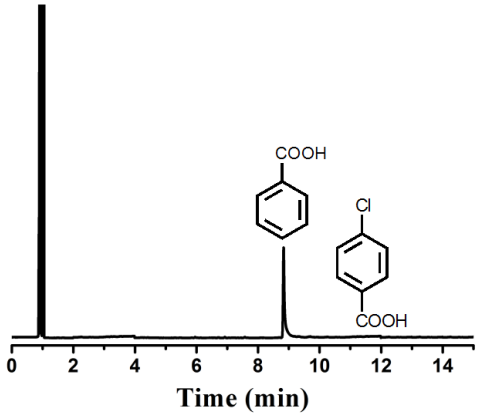

Fig. S60 GC analysis for the dechlorinating reaction of *p*-chlorbenzoic acid catalyzed by **Pd@TpTe-1** within 1.5 h in the batch experiment. The yield is 98%.

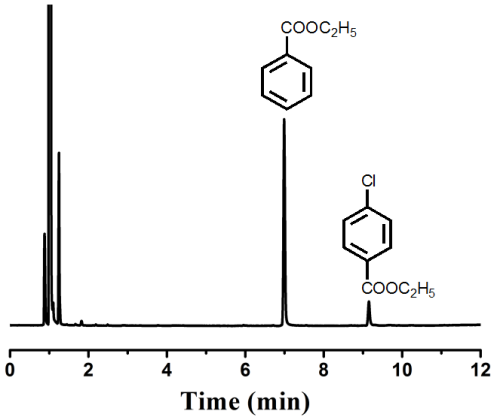

Fig. S61 GC analysis for the dechlorinating reaction of ethyl 4-chlorobenzoate catalyzed by **Pd@TpTe-1** within 6 h in the batch experiment. The yield is 93%.

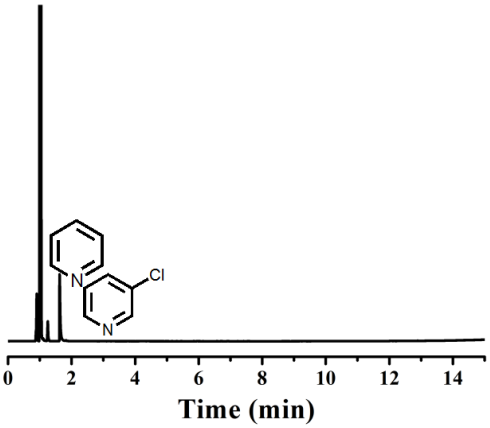

Fig. S62 GC analysis for the dechlorinating reaction of 3-chloropyridine catalyzed by **Pd@TpTe-1** within 3 h in the batch experiment. The yield is ≥99%.

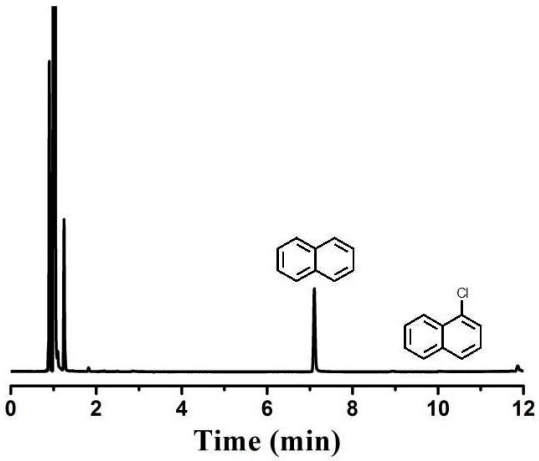

Fig. S63 GC analysis for the dechlorinating reaction of 1-chloronaphthalene catalyzed by **Pd@TpTe-1** within 6 h in the batch experiment. The yield is ≥99%.

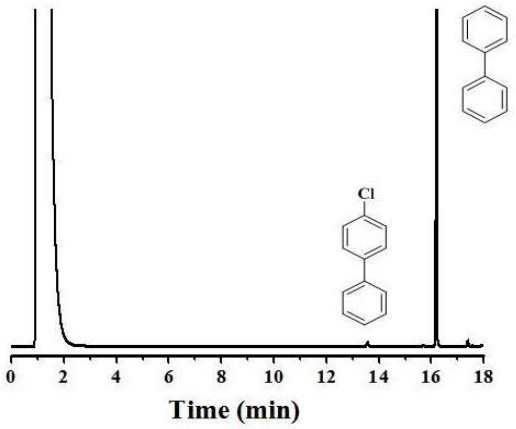

Fig. S64 GC analysis for the dechlorinating reaction of 4-chlorobiphenyl catalyzed by **Pd@TpTe-1** within 6 h in the batch experiment. The yield is 93%.

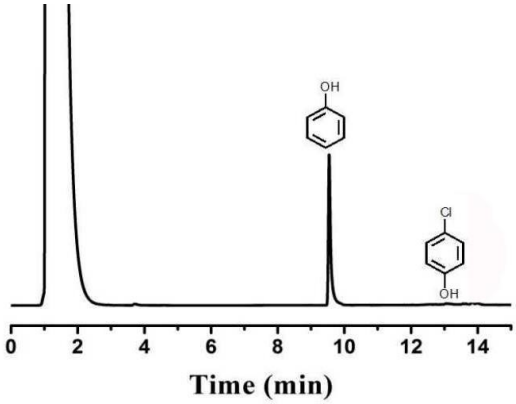

Fig. S65 GC analysis for the dechlorinating reaction of *p*-chlorophenol catalyzed by **Pd@TpTe-1@chitosan** within 2 h in the flow-through experiment for the first run. The yield is 98%.

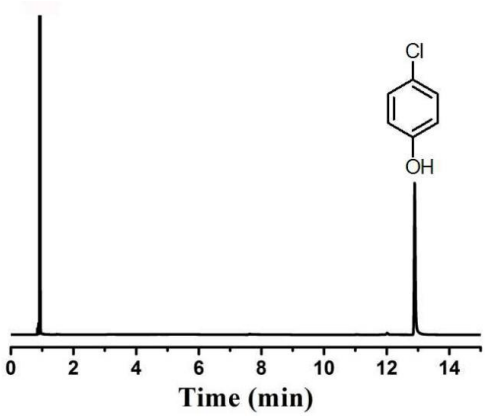

Fig. S66 GC analysis for the dechlorinating reaction of *p*-chlorophenol catalyzed by **TpTe-1@chitosan** within 2 h in the flow-through experiment. The yield is 0%.

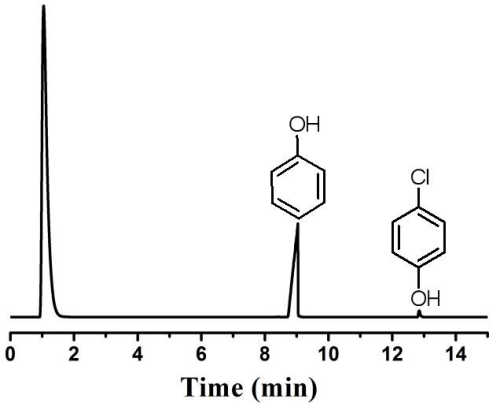

Fig. S67 GC analysis for the dechlorinating reaction of *p*-chlorophenol catalyzed by **Pd@TpTe-1@chitosan** within 2 h in the flow-through experiment for the second run. The yield is 97%.

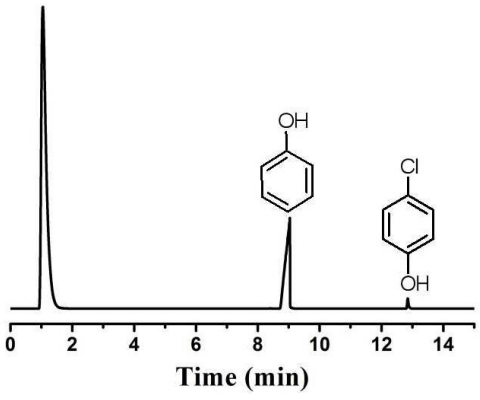

Fig. S68 GC analysis for the dechlorinating reaction of *p*-chlorophenol catalyzed by **Pd@TpTe-1@chitosan** within 2 h in the flow-through experiment for the third run. The yield is 96%.

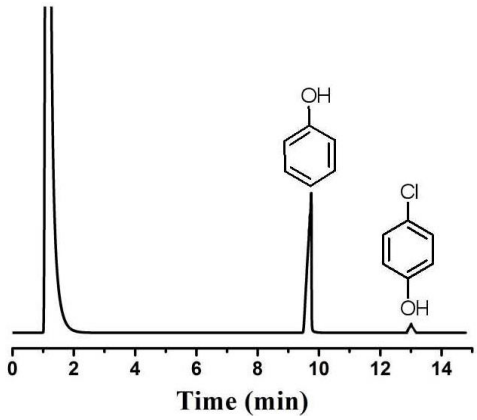

Fig. S69 GC analysis for the dechlorinating reaction of *p*-chlorophenol catalyzed by **Pd@TpTe-1@chitosan** within 2 h in the flow-through experiment for the fourth run. The yield is 94%.

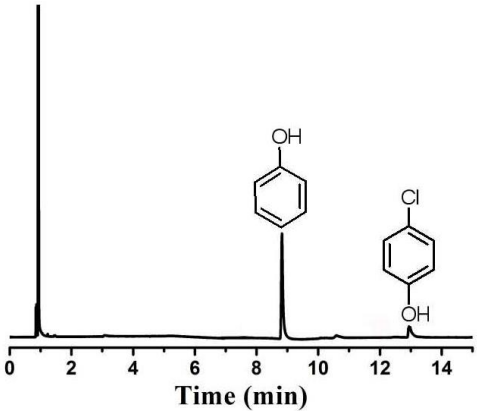

Fig. S70 GC analysis for the dechlorinating reaction of *p*-chlorophenol catalyzed by **Pd@TpTe-1@chitosan** within 2 h in the flow-through experiment for the fifth run. The yield is 93%.

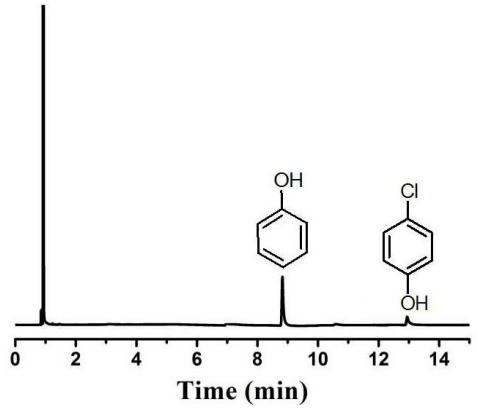

Fig. S71 GC analysis for the dechlorinating reaction of *p*-chlorophenol catalyzed by **Pd@chitosan** within 2 h in the flow-through experiment. The yield is 76%.

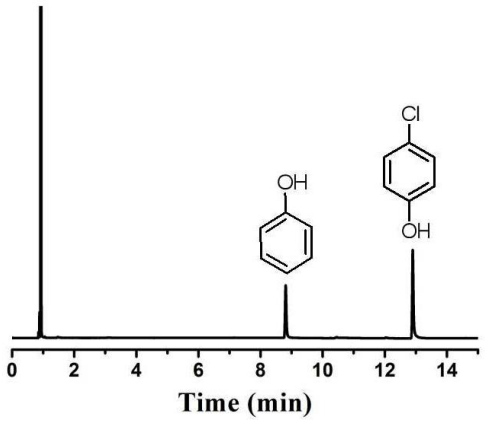

Fig. S72 GC analysis for the dechlorinating reaction of *p*-chlorophenol catalyzed by **Pd@chitosan** within 2 h in the flow-through experiment for the second. The yield is 43%.

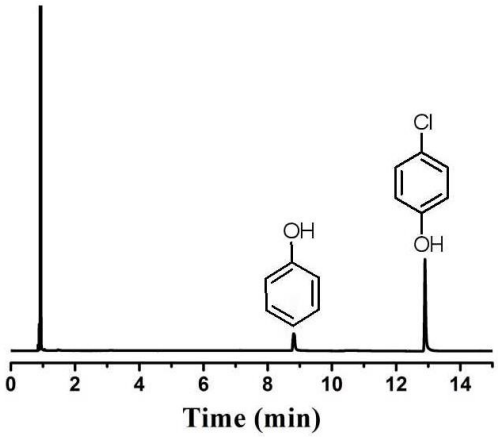

Fig. S73 GC analysis for the dechlorinating reaction of *p*-chlorophenol catalyzed by **Pd@chitosan** within 2 h in the flow-through experiment for the third run. The yield is 17%.

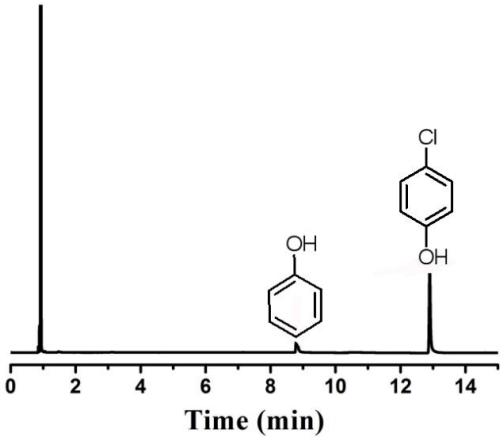

Fig. S74 GC analysis for the dechlorinating reaction of *p*-chlorophenol catalyzed by **Pd@chitosan** within 2 h in the flow-through experiment for the fourth run. The yield is 7%.

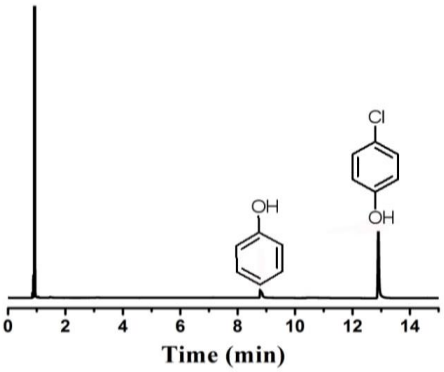

Fig. S75 GC analysis for the dechlorinating reaction of *p*-chlorophenol catalyzed by **Pd@chitosan** within 2 h in the flow-through experiment for the fifth. The yield is 3.5 %.

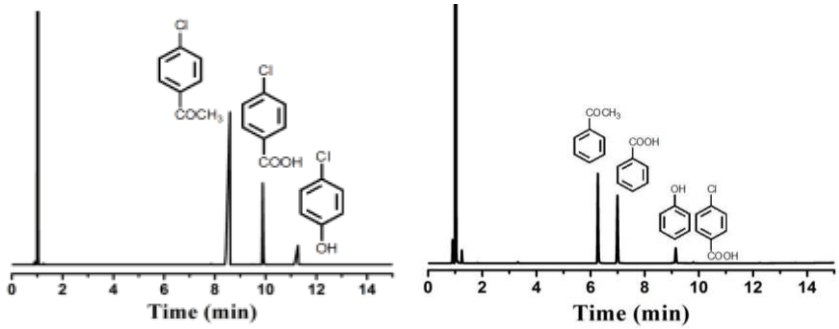

Fig. S76 GC analysis for the amplified dechlorination of three-component CBs via COF-based aerogel-connected flow-through microreactor within 10 h. Left: the GC spectra of reactant, Right: the GC spectra of the reaction product. The corresponding dechlorinating yield for *p*-chlorophenol, *p*-chlorbenzoic acid, and *p*-chloroacetophenone was 100 %, 99 %, and 100 % within 10 h based on GC analysis, respectively.

7. References

[1] S. Kandambeth, A. Mallick, Binit. Lukose, M. V. Mane, T. Heine, R. Banerjee, *J. Am. Chem. Soc.* 2012, **134**, 19524-19527.

[2] S. Chandra, S. Kandambeth, P. B. Biswal, B. Lukose, S. M. Kunjir, M. Chaudhary, R. Babarao, T. Heine, R. Banerjee, *J. Am. Chem. Soc.,* 2013, **135**, 17853-17861.

[3] a) Z. X. Kang, Y. W. Peng, Y. H. Qian, D. Q. Yuan, M. A. Addicoat, T. Heine, Z. G. Hu, L. Tee; Z. G. Guo, D. Zhao, *Chem. Mater*., 2016, **28**, 1277-1285. b) L. Stegbauer, M. W. Hahn, A. Jentys, G. Savasci, C. Ochsenfeld, J. A. Lercher, B. V. Lotsch, *Chem. Mater*., 2015, **27**, 7874−7881.

[4] G.-J. Chen, X.-B Li, C.-C Zhao, H.-C Ma, J.-L. Kan, Y.-B. Xin, C.-X. Chen, Y.-B. Dong, *Inorg. Chem.*, 2018, **57**, 2678-2685.